Clinical Neurophysiology 174 (2025) 131–147

Contents lists available at ScienceDirect

Clinical Neurophysiology

journal homepage: www.elsevier.com/locate/clinph

Electrophysiological hemispheric asymmetries induced by parietal stimulation eliciting visual percepts

D. Bonfanti [a], E. Bertacco [a], L.C. Parra [b], C. Mazzi [a,*,1], S. Savazzi [a,1]

[a] Perception and Awareness Lab, Department of Neuroscience, Biomedicine and Movement Sciences, University of Verona, Verona, Italy
[b] Department of Biomedical Engineering, City College of New York, New York, USA

ARTICLE INFO

Keywords:
TMS-EEG
Phosphenes
Intraparietal sulcus (IPS)
Hemispheric asymmetries
Two-streams hypothesis
Visual consciousness

ABSTRACT

Objective: We aimed to establish if the electrophysiological activity resulting from the direct stimulation of the intraparietal sulcus and eliciting visual percepts is hemispheric-specific.
Methods: We tested nineteen participants. Each received 360 TMS pulses at phosphene threshold intensity over right and left IPS while recording EEG. After each pulse, participants had to report if they had seen a phosphene.
Results: Parietal phosphene perception is associated with hemispheric-specific activations: phosphenes elicited by left TMS involve central and frontal electrodes at about 30 ms, and frontal, central and parieto-occipital electrodes from 120 to 250 ms; phosphenes elicited by right parietal TMS involve parietal and centro-parietal electrodes at about 60 ms, and frontal, central and parietal electrodes from 150 to 250 ms. Correlated Component Analysis shows that primary visual areas are not activated when phosphenes are produced by TMS over IPS.
Conclusions: Our results show that direct stimulation of IPS gives rise to sustained patterns of activity specific to the stimulated hemisphere. Moreover, elicited parietal phosphenes are associated with evoked activity specific to the stimulated hemisphere and located outside early visual processing areas.
Significance: This study highlights hemispheric differences in the electrophysiological dynamics related to parietal phosphenes, and shows that the dorsal pathway can give rise to visual conscious percepts.

1. Introduction

The posterior parietal cortex (PPC), centered around the intraparietal sulcus (IPS), has been associated with many functions (Xu Y., 2018): planning and controlling visually guided behavior to interact with the surrounding environment proficiently (Andersen & Cui, 2009; Culham & Valyear, 2006); attention, with PPC responding to salient and task-relevant stimuli, giving rise to a spatially organized priority map that can guide both visual and motor systems (Corbetta & Shulman, 2002; Parisi et al., 2020; Vossel et al., 2012); representation of spatial locations, with PPC hosting the presence of multiple spatial reference frames (e.g., head-centered or eye-centered), accompanied by the presence along IPS of topographic maps (Colby & Goldberg, 2003; Kravitz et al., 2011; Silver & Kastner, 2009).

For all these functions, hemispheric asymmetries have been detected. In the field of visual attention, numerous studies have reported distinct lateralization patterns. According to Kinsbourne's model, each hemisphere determines an attentional bias towards the contralateral visual hemifield, with the rightward bias determined by the left hemisphere being stronger than the leftward bias from the right hemisphere (Kinsbourne, 1977); this potentially explains the more frequent appearance of phenomena like neglect and extinction after a rightward parietal lesion. Later neuroimaging results pointed to the existence of two distinct attentional systems differently distributed across the two hemispheres: a bilateral dorsal network, in charge of voluntary deployment of attention, and a right ventral network dealing with reorientation to unexpected events (Corbetta et al., 2008). The use of transcranial magnetic stimulation (TMS) has also provided causal evidence supporting these hemispheric differences in attentional control (Duecker & Sack, 2015; Xu G. Q. et al., 2016). For example, Capotosto and colleagues (Capotosto et al., 2012) have demonstrated that repetitive TMS (rTMS) over the right IPS disrupts anticipatory modulation of alpha-band oscillations, leading to deficits in contralateral target detection. Moreover, Bien and colleagues (Bien et al., 2012) showed that

* Corresponding author.
E-mail address: chiara.mazzi@univr.it (C. Mazzi).
[1] These authors contributed equally.

https://doi.org/10.1016/j.clinph.2025.03.041
Accepted 31 March 2025
Available online 11 April 2025

right IPS stimulation produces more pronounced deficits in detecting contralesional stimuli when a competing ipsilesional stimulus is present, compared to left IPS stimulation. The existence of this dissociation between left and right IPS has been further confirmed in a recent meta-analysis (Wang T. et al., 2023), showing that inhibitory TMS on PPC has a different effect in the two hemispheres for the line bisection task and the landmark tasks: results are displaying a clear neglect-like effect after TMS on right PPC, which is basically absent after TMS of left PPC.

Hemispheric asymmetries have also been detected in how the two hemispheres process spatial information. For example, it is widely known that damage to the right inferior parietal lobule (IPL) can result in spatial neglect; however, damage to the homolog left IPL can result in ideomotor apraxia, characterized by a deficit in correctly imitating hand gestures and mimicking tool use (Husain & Nachev, 2007).

Action-related functions seem to present some degree of lateralization as well, with many functions being located in the dominant hemisphere. Early studies showed that the left IPS is involved in both perceiving goal-directed hand actions (Bonda et al., 1996) and action selection independently of the side of execution (Schluter et al., 2001). This has been further confirmed, showing the role that left parietal areas – including IPS – can have in the preparation and redirection of movements ("motor attention"), with left hemisphere stroke patients classically suffering from apraxic motor deficits (Rushworth et al., 2003). Lesions to PPC can also have a differential effect on adaptive visuomotor control, with deficits primarily observed after left-sided damage (Mutha et al., 2011). Another study on stroke patients showed that grasping and estimation illusions were better dissociated in the performance of left stroke patients while being of similar size in right stroke patients: this points to differently lateralized interactions between visuomotor and visuoperceptual streams in the two hemispheres, with them being more dissociated in the left hemisphere (Radoeva et al., 2005).

These hemispheric differences also extend to white matter tracts connecting IPS with prefrontal regions: in the context of movement execution, they correlate differently with different aspects of kinematic data (Budisavljevic et al., 2017). Moreover, the anterior part of IPS (aIPS) in both hemispheres has also been associated with parietal premotor activity, highlighting how this portion of IPS is specialized for hand movements directed toward the contralateral space (Di Russo et al., 2016; Sulpizio et al., 2017).

Recently, evidence has emerged that areas along IPS are also capable of processing action-independent nonspatial visual information, undermining the rigid functional division posed by the two-streams model (Xu Y., 2018) proposed by Ungerleider and Mishkin (Ungerleider & Mishkin, 1982) and updated by Goodale and Milner (Goodale & Milner, 1992). While both streams receive their inputs mainly from the striate cortex (although the dorsal stream receives at least part of it through a subcortical route (Whitwell et al., 2020), the pathways that they follow are separate with a ventral one proceeding towards the inferotemporal cortex, and a dorsal one reaching the posterior parietal areas. The distinction is also functional: the ventral stream plays a significant role in the conscious identification of objects while the dorsal stream is linked with visuomotor guidance of actions, being responsible for nonconscious sensorimotor transformations.

This distinction originates from neuropsychological findings of a double dissociation between optic ataxia, a visuomotor deficit caused by damage to the dorsal stream, and visual agnosia, a visual recognition deficit caused by damage to the ventral stream. Over the years, however, this double dissociation has been questioned, as both these neurological conditions show traits and characteristics typically associated with the other one, i.e., ventral damage can impoverish visually guided behavior, and dorsal damage can impair visual perception (Pisella et al., 2006; Rossetti & Pisella, 2018). Furthermore, different kinds of agnosia predominantly manifest in a lateralized fashion: while associative agnosia is predominantly caused by left hemispheric damage, apperceptive agnosia follows a right hemispheric lesion (de Renzi, 1969; de Renzi & Spinnler, 1966; Ferro & Santos, 1984; Warrington & Taylor, 1973). Of importance for the present paper, lesion studies in ataxic and agnosic patients show not only the existence of perceptual characteristics in the dorsal stream but also that these latter present a certain degree of hemispheric lateralization.

Concurrently, neuroimaging studies have shown that dorsal areas can exhibit adaption to novel and familiar objects, while also displaying tolerance to changes in size and viewpoints similarly to what happens in ventral regions (Konen & Kastner, 2008); moreover, they can hold distinctive representations for low-, mid- and high-level visual features, displaying processing characteristics similar to the ones shown by ventral object-processing regions (Jeong & Xu, 2016). These results highlight the involvement of IPS in visual processing, in a way that is independent from other functions classically associated with IPS.

Another line of research has successfully proved that areas located along IPS can carry on perceptual processing of visual information by being capable of giving rise to visual percepts under specific conditions. Marzi and colleagues (Marzi et al., 2009), in a TMS experiment, have been the first to find that stimulation of IPS can elicit phosphenes (i.e., visual percepts in the absence of any external visual stimuli), similar to what happens when stimulating early ventral visual areas. This finding, replicated in many other studies (Bagattini et al., 2015; Fried et al., 2011; Mazzi et al., 2014; Samaha et al., 2017; Tapia et al., 2014) has started to reveal that even the dorsal stream has the potential to produce conscious visual perceptions, further adding to the idea that a subdivision between a conscious ventral stream and an unconscious dorsal stream might be too simplistic.

While these findings support a role for IPS in perceptual processing, most studies have focused on the left parietal cortex, leaving open the question of whether right and left IPS contribute similarly to visual awareness. Therefore, this work aims to determine if IPS asymmetries between the two hemispheres extend to visual perception. To do so, we performed a TMS-EEG study stimulating left and right IPS at phosphene threshold (PT). The EEG activity elicited from phosphene perception was then compared across the two stimulated sites, to detect possible hemispheric differences in the neural dynamics that give rise to visual awareness.

2. Materials and methods

2.1. Participants

A total of 90 volunteers were screened during the training phase for the perception of consistent parietal phosphenes (see below, Section 2.4 "Experimental procedure"). Participants not reporting any parietal phosphenes or perceiving them inconsistently or rarely were not considered for the experimental sessions (Kammer et al., 2005; Mazzi et al., 2014). In the end, 23 right-handed volunteers (3 males, mean age 22.73±2.52) with normal or corrected-to-normal vision participated in the study and were reimbursed for their participation. Data from four participants were excluded because the stimulated areas during the experimental sessions were partially located in the occipital lobe. Written informed consent was obtained from participants according to the 2013 Declaration of Helsinki. The experimental protocol has been approved by the local Ethics Committee. Participants underwent a screening questionnaire (adapted from Rossi et al., 2009) addressing risk factors associated with TMS; no participant reported any contraindications.

2.2. MRI image acquisition

We acquired MRI images from seven participants. They underwent MRI with a 1.5 Tesla scanner with a 15-channel head coil (Philips Ingenia, Philips Healthcare, Eindhoven, The Netherlands) at the Borgo Roma Hospital in Verona. We acquired a whole-brain high-resolution 3D T1-weighted image with magnetization-prepared rapid acquisition gradient echo (MPRAGE) (TR 7.7 ms/TE 3.5).

2.3. Transcranial magnetic stimulation protocol

Single-pulse magnetic stimulation via a 70 mm figure-of-eight coil connected with a Magstim Rapid2 system (maximum output 2.2 T, Magstim Company Limited, Whitland, UK). TMS coil was placed tangentially to the scalp surface, keeping the handle upward to avoid unwanted activations of neck and shoulder muscles.

We used a neuronavigation software (SofTaxic, E.M.S., Bologna, Italy) combined with a 3D optical digitizer (Polaris Vicra, NDI, Waterloo, Canada) to control for possible coil displacements within a 2 mm accuracy threshold and to verify the stimulation target.

The location of stimulation sites was performed through suprathreshold phosphene induction within a circle of 2 cm in diameter centered on electrodes P3 (left hemisphere) and P4 (right hemisphere) of the 10-20 EEG system (Mazzi et al., 2014). Neuronavigation based on individual MRI images, when available, was used to constantly check that the focus of the stimulation was aimed at the IPS; when this was not the case, an MNI-based template was employed in the neuronavigation software.

We used the "Method of Constant Stimuli" (MOCS) (Mazzi et al., 2017b) to establish the individual phosphene threshold (PT) for the two stimulation sites. We took the intensity at which participants perceived phosphenes in 50% of trials as the PT and used it as stimulation intensity during the experiment. In the course of the experiment, the stimulation intensity was adjusted as needed to keep the percentage of reported phosphenes at 50%.

2.4. Experimental procedure

Participants sat in a dark room in front of a 17in. LCD monitor at 57 cm. Their head was secured in a chin rest to keep their eyes aligned with the screen center, on which participants were instructed to maintain their fixation during the experiment.

Before the experiment, we conducted a training session during which participants received a brief explanation of the nature and characteristics of phosphenes, after which they were tested for the perception of phosphenes.

Each experimental session started with the localization of the stimulation hotspot for both IPS; we then used the MOCS method to establish the PT to use as stimulation intensity for each stimulation site. Finally, we performed the actual experiment. The order of stimulations in each of these steps was counterbalanced across participants (Fig. 1A).

Participants had to report, for each TMS pulse, the presence or absence of a phosphene by pressing the keyboard keys *m* (right hand) or *z* (left hand), with the responses counterbalanced across participants. They underwent two consecutive sessions comprising six blocks of 60 stimulations each, for a total of 360 TMS pulses per stimulation site. Each trial started with a random interval of 700-1000 ms, at the end of which a single pulse of TMS was administered. After that, participants had up to 2000 ms to report on the presence/absence of the phosphene by pressing the proper key; once this was done, an inter-trial interval of 1400 ms separated this trial from the following one (Fig. 1B). For the entire duration of the experiment, each participant wore earplugs playing white noise to help mask the auditory co-stimulation associated with each TMS pulse.

2.5. EEG recording and preprocessing

TMS-compatible EEG equipment (BrainAmp, Brain Products GmbH, Munich, Germany) was used to record EEG activity (BrainVision Recorder), in combination with a Fast'n East cap with 59 TMS-compatible Ag/AgCl pellet pin electrodes (EasyCap GmbH, Herrsching, Germany) positioned according to the 10-20 International System. We employed additional electrodes as online reference (RM), ground (AFz) and to control horizontal and vertical eye movements. We kept electrode impedance below 5 KΩ.

We positioned a custom-made polystyrene C-shaped annulus over the nearest electrode targeted by TMS to enable reliable EEG recording from it and to reduce TMS-related artifacts (Bagattini et al., 2015).

EEG preprocessing was based on custom scripts following a previously published pipeline specifically devised to analyze TMS-EEG data and remove TMS-related artifacts (Bertazzoli et al., 2021; Fulvio et al., 2024; Rogasch et al., 2017). The EEG signal was processed offline with Matlab 2021b (Mathworks, USA), the EEGLAB toolbox (version 2021.0, Delorme & Makeig, 2004), and the TMS-EEG signal analyzer (TESA) extension (Rogasch et al., 2017). The continuous raw signal, digitized at 5000 Hz, was cut 1000 ms before and after the TMS pulse. Demeaning was performed on epoched data using the whole epoch. The TMS pulse artifact was removed from -2 to 10 ms and replaced with cubic interpolation to avoid ringing artifacts. Data were then downsampled at 500 Hz. Independent component analysis (ICA) (Delorme et al., 2007) was then used to remove the tail-end of the muscle artifact due to the TMS pulse (Rogasch et al., 2014, Rogasch et al., 2017). In this first run of ICA, an average of 1±0.74 components were removed from P3 datasets, and

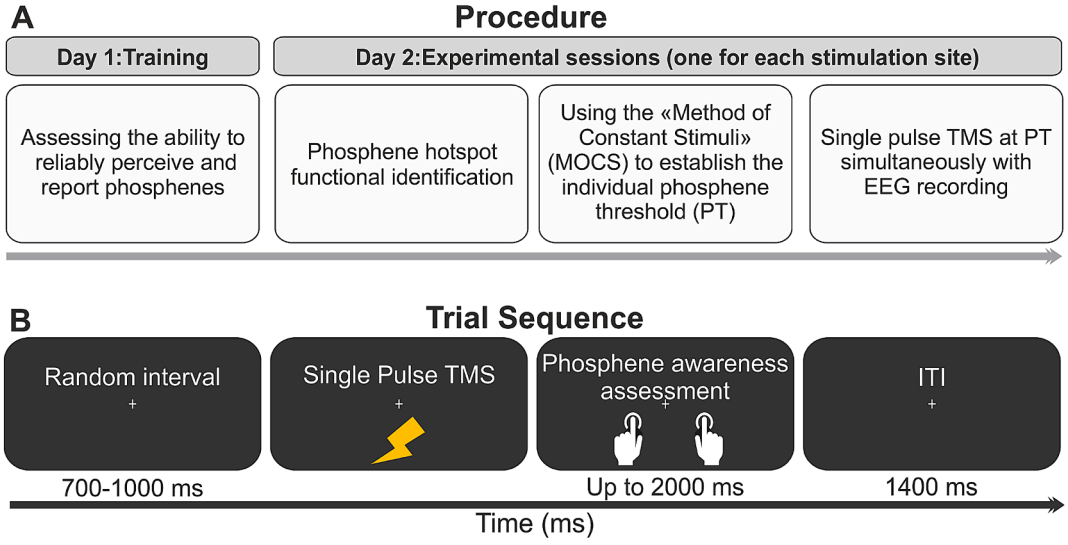

Fig. 1. Experimental procedure and trial sequence for the experiment. A: Outline of the experimental steps followed for each participant. B: Timing of each experimental trial.

an average of 0.94±0.97 components were removed from P4 datasets. A paired t-test showed no significant differences in the number of removed components [t(1,18) = 0.369; p = 0.716, Cohen's d = 0.08]. Subsequently, we applied a bandpass filter (0.1-100 Hz, zero-phase, fourth-order Butterworth band-pass) and band-stop filter (49-51 Hz). We performed a second run of ICA to check for blinks, lateral eye movements (saccades), persistent muscle activity, and electrode noise. After the second run of ICA, an average of 27.57±6.06 components were removed from P3 datasets, and an average of 27.42±6.2 components were removed from P4 datasets. A paired t-test showed no significant differences in the number of removed components [t(1,18) = 0.163; p = 0.872, Cohen's d = 0.03]. Before each ICA round, interpolated data from -2 to 10 ms were substituted with constant amplitude values and then interpolated again to improve component decomposition. We then re-referenced data to a point at infinity (Yao, 2001) using the REST toolbox (Dong et al., 2017). Finally, we low-pass filtered the data at 40 Hz and epoched them from -100 to 500 ms. Datasets from the P4 stimulation session were flipped in order to overlap the stimulation sites in the two experimental sessions. Datasets from both hemispheres were then merged and downsampled at 250 Hz. We used TBT toolbox (Ben-Shachar, 2020) to detect and reject bad trials. Baseline correction was finally performed from -100 to 0 ms.

For each participant, we then computed the Local Mean Field Power (LMFP) (Lehmann & Skrandies, 1980) for the two hemispheres, considering ipsilateral and contralateral channels to the stimulation; midline electrodes were not included in the calculation.

2.6. Correlated component analysis

Inter-subject correlation of EEG responses to TMS was measured via correlated component analysis (CorrCA) (Parra et al., 2018), a technique first introduced by Dmochowski et al. (Dmochowski et al., 2012). The code used to perform CorrCA on our data has been previously published by Parra Lab (https://www.parralab.org/isc/).

CorrCA is a backward model that captures shared sources of covariation in the data: it does so by defining a model comprised of several projection vectors (components) that linearly combine electrodes and on which the data is projected, resulting in the isolation of significant correlation between subjects in the data. In this way, our EEG data – characterized by high dimensionality – are reduced to a few components with minimal correlation in time and maximal correlation across participants. Backprojecting the resulting components on the data gives us their specific time course for each condition: this allows us to compare and see how the shared activity is influenced by the different experimental conditions.

To do so, we removed the stimulated electrode from our flipped data (i.e., the electrode P3) to avoid distortions in the decomposition due to the presence of the TMS pulse. Then, trials belonging to all four different conditions (*Stimulation site* [P3|P4] x *Phosphene awareness* [present|absent]) were averaged for each subject and concatenated along the time dimension. CorrCA analysis was then performed on the combined data from all subjects, determining a set of components that capture the maximum correlation across time samples between the 19 subjects. The statistical significance of the detected components was assessed via random circular shuffle (200 repetitions) (Parra et al., 2018). Circular shuffle means that the signal of each subject is shifted in time by a random time delay, such that multiple subjects are no longer temporally aligned to one another. Any temporal correlation between subjects is, therefore, entirely accidental. Inter-subject correlation measured on such random-shifted data thus provides a distribution under the null hypothesis of no inter-subject correlation. Its circularity derives from the fact that, when shifting in time, the data samples at the end/beginning of the sequence are wrapped around to appear at the beginning/end.

We then projected the weights of the backward model that we obtained on the averaged flipped data separately for each of the four conditions to compute the significant correlated components for each condition and allow statistical comparison between them.

2.7. Source localization

To deduce cortical electrical activity from EEG signals recorded on the scalp, we employed exact low-resolution brain electromagnetic tomography (eLORETA) as a source estimation model. eLORETA is a linear inverse solution that estimates cortical electrical activity from EEG data with exact localization, although with low spatial resolution (Grech et al., 2008; Jatoi et al., 2014; Pascual-Marqui, 2007; Pascual-Marqui et al., 2011). It represents cortical electrical activity on a realistic head model (standardized scalp-skull-brain head model) (Fuchs et al., 2002) based on MNI152 template (Mazziotta et al., 2001). eLORETA provides a 3D solution space made of 6239 voxels in the cortical grey matter, with a spatial resolution of 5x5x5 m^3.

To perform source localization, we used the freeware available at https://www.uzh.ch/keyinst/loreta (version 4.11.2008). EEG data were average referenced, and Talairach coordinates were created for all electrodes following a template of the 10-20 electrode system (Jurcak et al., 2007). Electrode coordinates and MNI152 head model were then employed to determine the transformation matrix, with the aim of converting scalp electric potential differences to brain current densities.

We used eLORETA on our TEP data to localize the cortical sources associated with the different conditions. We also applied eLORETA on the forward models of the significant components we obtained from CorrCA, to translate them into the corresponding distributions of underlying cortical activity (Dmochowski et al., 2012).

2.8. Statistical analyses

2.8.1. Behavioral Statistics

JASP was used to analyze behavioral data (JASP Team, 2020). Trials with reaction times (RTs) <150 ms or >3 SD were considered outliers and excluded from further analysis. A t-test was conducted on the stimulation intensity necessary to find PT in the two stimulated sites, to check for possible hemispheric differences. We then performed a one-sample t-test to check if the percentages of positive and negative answers differed from a 50% value. A 2x2 repeated-measures ANOVA with *Stimulation site* (P3|P4) and *Phosphene awareness* (present|absent) as within-subject factors was used to analyze RTs.

2.8.2. LMFP Statistics

A series of 2x2 ANOVA with *Stimulation site* (P3|P4) and *Stimulated hemisphere* (ipsilateral|contralateral) as within-subject factors was carried out on LMFPs for each time point. False Discovery Rate (FDR) (Groppe et al., 2011) was used to control for multiple comparisons.

2.8.3. TEPs statistics

LIMO EEG toolbox was used for TMS-EEG data analysis (Pernet et al., 2011). We performed a 2x2 ANOVA with *Stimulation site* and *Phosphene awareness* as within-subject factors on TMS-evoked potentials (TEPs), followed by t-tests to study the factors' interaction. We then thresholded results by applying a temporal filter that revealed only significant activations whose duration was at least 12 ms. Clusters of significant electrodes were identified around the peaks in GMFP waveforms, calculated separately for each statistical comparison.

2.8.4. CorrCA statistics

For each significant CorrCA component we performed a 2x2 ANOVA with *Stimulation site* and *Phosphene awareness* as within-subject factors on the backprojected components weights on the four conditions. FDR was used to control for multiple comparisons.

3. Results

3.1. Behavioral results

The mean PT for the two stimulation sites was 74.5% of maximum stimulator output for P3 stimulation site, and 75.1% for P4 stimulation site (Fig. 2). These two values were not statistically different [t(18) = -0.531; p = 0.602]. The mean percentages of detected phosphenes were 37.5% after P3 stimulation and 32.8% after P4 stimulation (Fig. 3A).

A 2-way repeated measure ANOVA conducted on RTs showed a significant effect of *phosphene awareness* [F(1,18) = 4.661; $p < 0.05$; $\eta_p^2 = 0.206$], with positive phosphene reports (976 ms for P3 and 990 ms for P4) being significantly slower than negative reports (947 ms for P3 and 924 ms for P4). This might be explained by the nature of parietal phosphenes, which in literature are described as weaker and fainter than occipital ones (Mazzi et al., 2014): participants might have needed, therefore, more time to realize that they had perceived something, increasing the amount of time needed to confirm a positive report. Neither the *Stimulation site* [F(1,18) = 0.01; p = 0.921; $\eta_p^2 = 5.608e\text{-}4$] nor the interaction [F(1,18) = 3.757; p = 0.068; $\eta_p^2 = 0.173$] were significant (Fig. 3B).

3.2. LMFP results

The analysis performed over LMFP data detected a significant effect of the *Stimulated hemisphere* (ipsilateral|contralateral) in the time range between 12 to 104 ms [all ps < .05]. No significant differences were found for both the *Stimulation site* and the interaction between the two factors (Fig. 3C).

3.3. TEP results

Fig. 4A includes the butterfly plots associated with the two *Stimulation site* conditions (P3|P4), together with the topographies and source reconstructions related to the TEP peaks. Particularly, concerning source reconstructions in the P3 condition, the cortical generator for the first peak at 36 ms was located in Brodmann Area (BA) 7 within the precuneus (MNI coordinates: X= -5; Y= -65; Z= 65), while the cortical generator for the peaks at 56 ms, 76 ms, 112 ms, and 164 ms was located in BA 5, in the postcentral gyrus (MNI coordinates: X= -20; Y= -50; Z= 70). With regard to source reconstructions in the P4 condition, the cortical generator for the first (36 ms) and second peak (56 ms) was located in BA7, in the postcentral gyrus (MNI coordinates for 36 ms peak: X= 25; Y= -55; Z= 70; MNI coordinates for 56 ms peak X= 20; Y= -55; Z= 70). The cortical generator of the third peak at 76 ms was located in BA7, in the superior parietal lobule (MNI coordinates: X= 25; Y= -65; Z= 65). The generator of the fourth peak (112 ms) was again located in BA7, in the postcentral gyrus, similarly to the first and second peaks (MNI coordinates: X= 25; Y= -55; Z= 70). The generator of the fifth peak (164 ms) was again in the superior parietal lobule (BA7), similarly to the third peak (MNI coordinates: X= 25; Y= -65; Z= 65). To report significant TEP activations, we identified temporal clusters based on GMFP peaks. A two-way repeated measures ANOVA on TEPs revealed a significant effect of *Stimulation site* [all ps < 0.05]. We found three main clusters: the first one in the 20-48 ms time window involved mainly frontal electrodes; the second, in the 48-100 ms time window, involved mainly fronto-central electrodes contralateral to stimulation; the third one in the 120-250 ms time window, involved mainly frontal electrodes contralateral to stimulation and bilateral central electrodes (Fig. 4B).

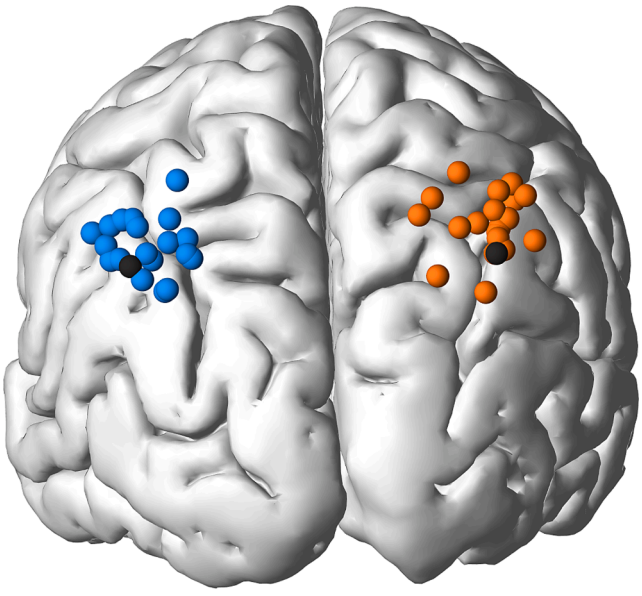

Fig. 2. Stimulation sites for each participant in the two hemispheres. Each dot corresponds to phosphene hotspot from a single participant for the specific hemisphere. Blue dots represent left TMS targets, while orange dots represent right TMS targets. Black dots correspond, respectively, to the P3 (left) and P4 (right) electrode positions.

Fig. 5A shows the butterfly plots related to the two *Phosphene awareness* conditions (present|absent), with the topographies and source reconstructions of the TEP peaks.

Source reconstruction for the "phosphene present" and "phosphene absent" conditions revealed that, for both conditions, the cortical generator of the peaks at 36 ms, 56 ms, 76 ms, 112 ms, and 160 ms were located in BA 7, in the superior parietal lobule (MNI coordinates: X= -30; Y= -65; Z= 60). Two different clusters were identified for *Phosphene awareness*: the first one, in the 100-120 ms time window, involved mainly fronto-central and parieto-occipital electrodes ipsilateral to the stimulation; the second, in the 120-250 ms time window, involved bilateral frontal, central, and parieto-occipital electrodes (Fig. 5B).

Considering the interaction between the two factors, we detected four clusters: the first in the 20-48 ms time window, involved bilateral centro-parietal electrodes; the second in the 48-100 ms time window, involved mainly bilateral frontal and centro-parietal electrodes; the third in the 100-124 ms time window, involved left fronto-central electrodes; the fourth in the 124-250 ms time window involved mainly bilateral fronto-central electrodes (Fig. 6).

The butterfly plots, together with the topographies and source reconstructions of the TEP peaks for "phosphene present" and "phosphene absent" conditions after left TMS, are shown in Fig. 7A. Source reconstruction for "phosphene present – left TMS" showed that the cortical generator of the peak at 36 ms was located in BA7, in the precuneus (MNI coordinates: X= -5; Y= -65; Z= 65), while the generator for the peaks at 56 ms, 76 ms, 112 ms was in BA 5, in the postcentral gyrus (MNI coordinates for 56 ms, 76 ms and 112 ms peaks: X= -20; Y= -50; Z= 70; MNI coordinates for 164 ms peak: X= -25; Y= -50; Z= 70). On the other hand, for "phosphene absent – left TMS" the cortical generator of the peak at 36 ms was in BA7, in the precuneus (MNI coordinates: X= -5; Y= -65; Z= 65), while the sources of the remaining peaks (56, 76, 112, and 160 ms) were all located in BA 5, in the postcentral gyrus (MNI coordinates: X= -20; Y= -50; Z= 70). In order to disentangle the contribution that the different factors gave in the interaction, we looked at the t-tests to check for the awareness-related activations in the two stimulation sites. When contrasting "phosphene present" vs. "phosphene absent" conditions after left IPS stimulation, we found two clusters: the first in the 20-44 ms time window involved mainly right fronto-central electrodes; the second, in the 116-250 ms time window involved bilateral frontal, central and parieto-occipital electrodes (Fig. 7B).

With regards to the right IPS stimulation, Fig. 8A shows the butterfly plots with the associated topographies and source reconstructions for "phosphene present" and "phosphene absent" conditions after right TMS. Source reconstruction for "phosphene present – right TMS"

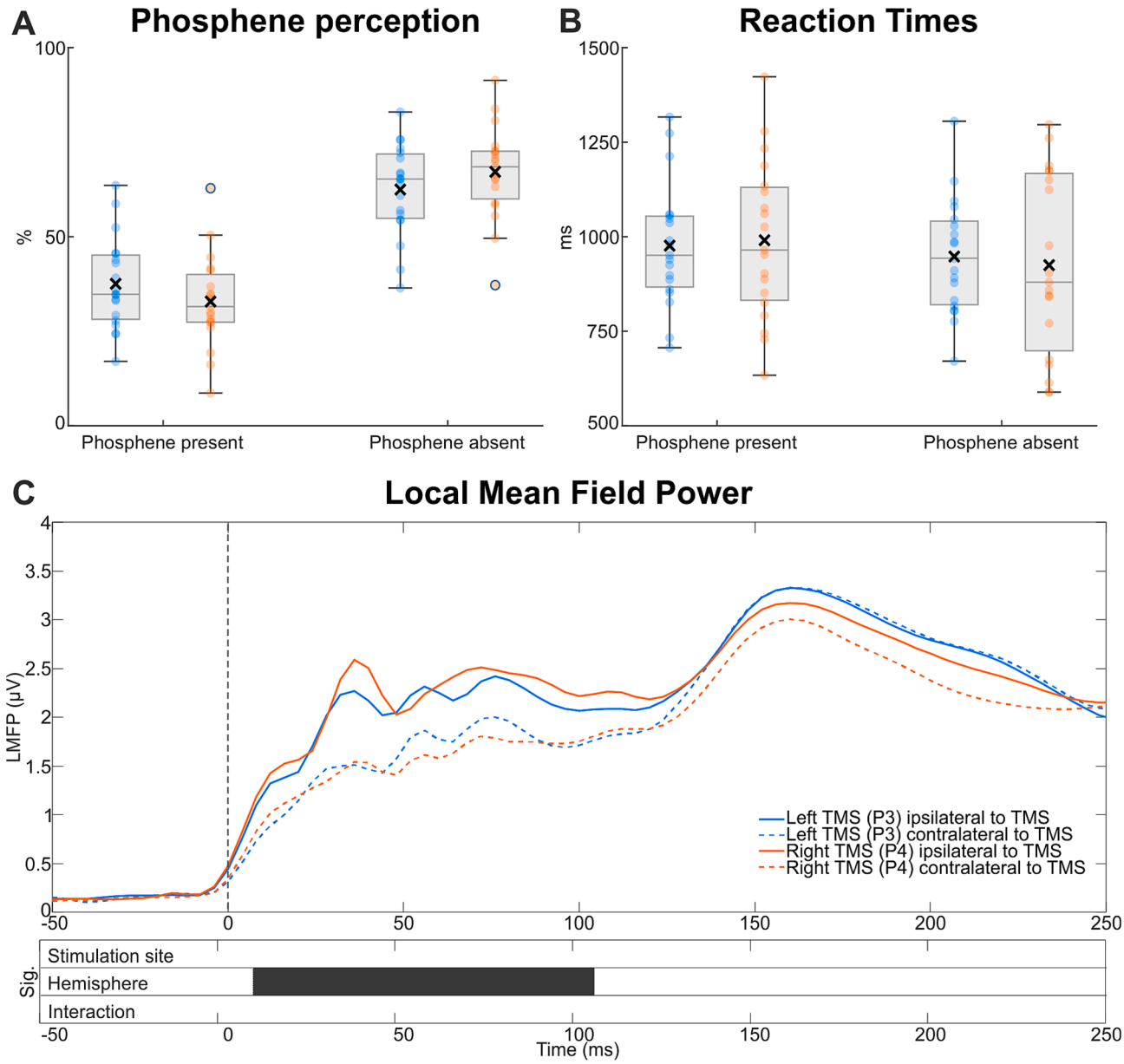

Fig. 3. Behavioral and LMFP results. A: Percentages of reported phosphenes for the two stimulated sites (blue for P3/left, orange for P4/right). Black Xs represent the mean value of the distribution, while colored dots represent individual data. B: Reaction times for "Phosphene present" and "Phosphene absent" trials for the two stimulation sites (blue for P3/left, orange for P4/right). Black Xs represent the mean value of the distribution, while colored dots represent individual data. C: LMFP calculated separately for each stimulation site, for both electrodes ipsilateral and contralateral to the stimulation (vertical midline electrodes not included). Gray bars below the plot represent the significant time intervals for each factor.

revealed that the cortical generator for the 36 ms and 56 ms peaks was BA 7, in the postcentral gyrus (MNI coordinates for 36 ms peak: X= 25; Y= -55; Z= 70; MNI coordinates for 56 ms peak: X= 20; Y= -55; Z= 70); the generator for the 72 ms peak was again BA 7, in the superior parietal lobule (MNI coordinates: X= 25; Y= -65; Z= 65). The sources of the 112 ms and 160 ms peaks were again located in BA 7, the first in the postcentral gyrus (MNI coordinates: X= 25; Y= -55; Z= 70), and the second in the superior parietal lobule (MNI coordinates: X= 25; Y= -65; Z= 65). On the other side, source reconstruction for the "phosphene absent – right TMS" condition shows that the generators of all the peaks are located in BA 7: for the 36 ms and 56 ms peaks, they are in the postcentral gyrus (MNI coordinates for 36 ms peak: X= 25; Y= -55; Z= 70; MNI coordinates for 56 ms peak: X= 20; Y= -55; Z= 70); the source of the 72 ms peak is in the superior parietal lobule (MNI coordinates: X= 25; Y= -65; Z= 65); the 112 ms peak originates again in the postcentral gyrus (MNI coordinates: X= 25; Y= -55; Z= 70), while the generator for the 160 ms peak is once more in the superior parietal lobule (MNI coordinates: X= 25; Y= -65; Z= 65). For right TMS, two clusters emerged from contrasting "phosphene present" vs. "phosphene absent" conditions: the first was located in the 48-100 ms time window, involving mainly left centro-parietal electrodes; the second between 124 and 250 ms, comprising bilateral frontal, central and parietal electrodes (Fig. 8B).

3.4. Correlated component analysis

CorrCA analysis revealed five significant correlated components across our dataset (Fig. 9, left). The first one exhibited a dipole with the positivity located over centro-frontal electrodes (mainly spread on the side ipsilateral to stimulation) and the negativity over parieto-occipital

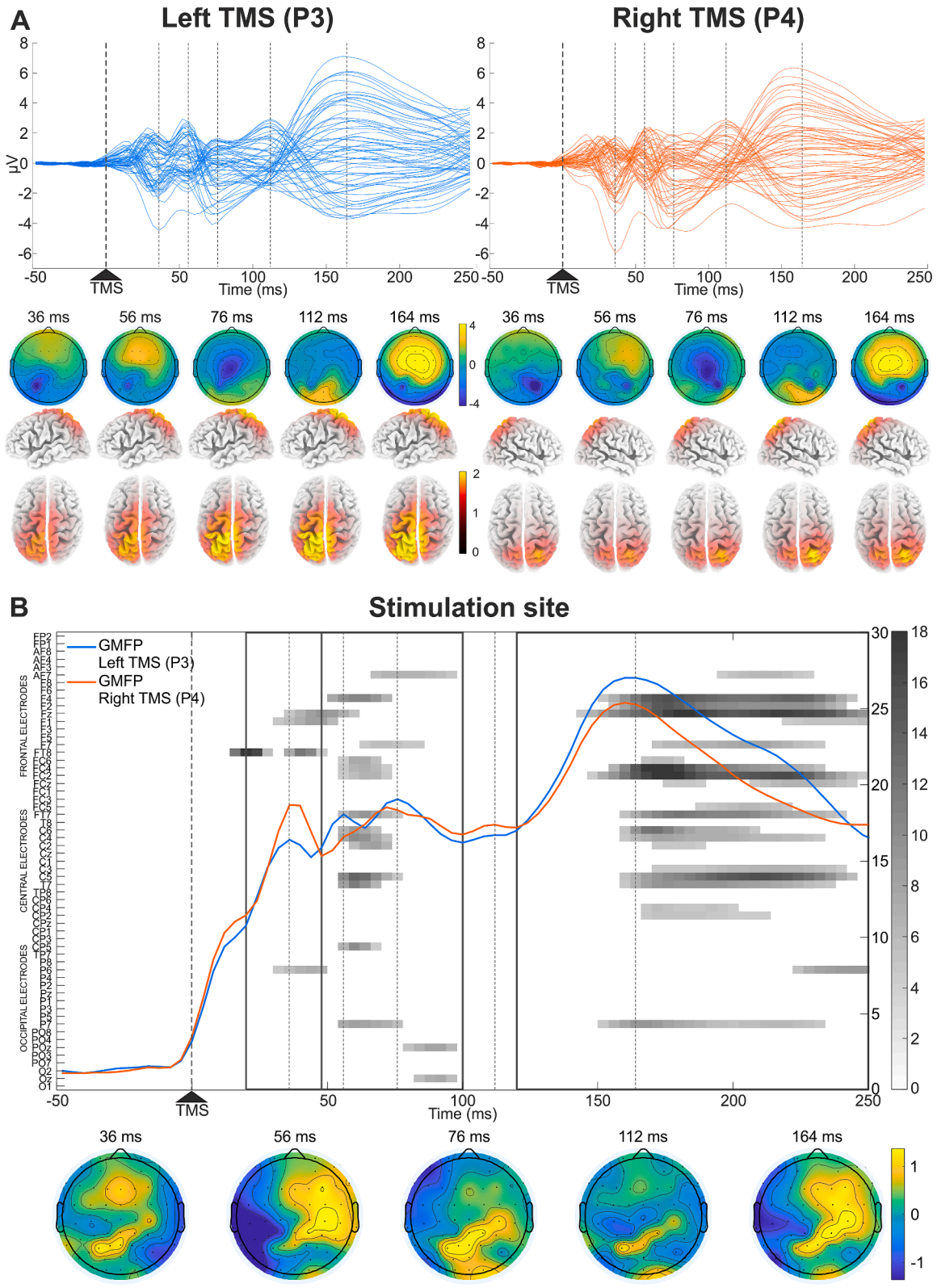

Fig. 4. Results from the ANOVA conducted on TEPs: main effects of *Stimulation site*. A: Butterfly plots depicting TEPs for the two conditions ("Left TMS", blue; "Right TMS," orange). Vertical dotted lines highlight the peaks of the different components, as determined by GMFP below. The topographies below represent the scalp distribution for each component, with corresponding source reconstruction. B: Raster plot depicting for each time point and each electrode the significant differences (expressed in F-values) between left and right TMS. Right TMS data were flipped so that stimulation sites overlapped. X and Y axes represent, respectively, time in milliseconds and electrodes (from posterior to anterior ones). The two lines superimposed represent the GMFPs associated with the two conditions, whose peaks were used to identify TEPs clusters. The vertical dotted lines highlight GMFP peaks. The scalp topographies represent scalp differences between the two conditions ("Right TMS" – "Left TMS"; "Right TMS" topographies were flipped to keep the stimulation site constant across the two conditions), with each map corresponding to the latency of each GMFP peak.

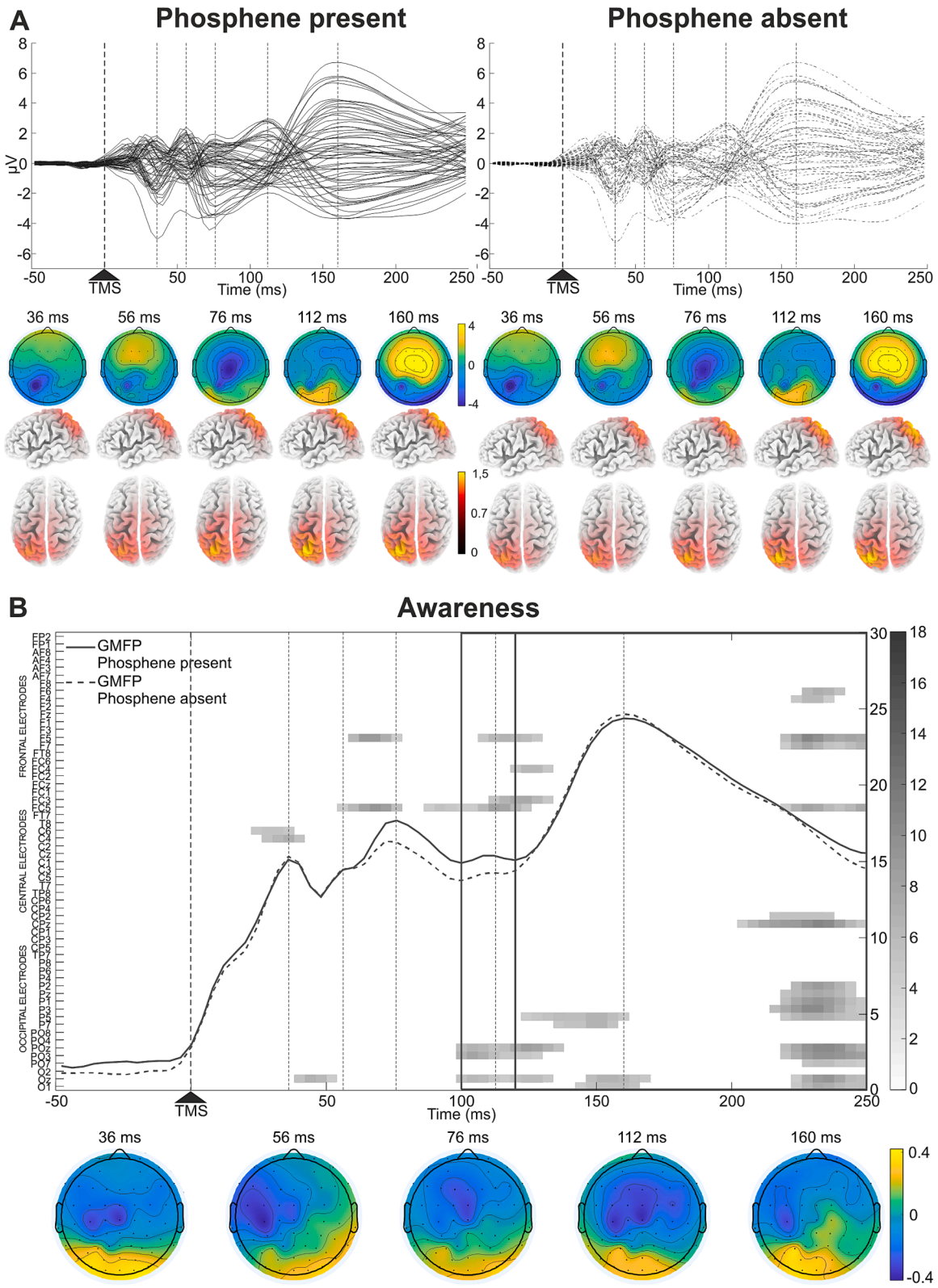

Fig. 5. Results from the ANOVA conducted on TEPs: main effects of *Phosphene awareness*. A: Butterfly plots depicting TEPs for the two conditions ("Phosphene present", continuous line; "Phosphene absent", dotted line). Vertical dotted lines highlight the peaks of the different components, as determined by GMFP below. The topographies below represent the scalp distribution for each component, with corresponding source reconstruction. Topographies have been flipped, so that stimulation site is always located on left IPS, in correspondence with P3 electrode. B: Raster plot depicting for each time point and each electrode the significant differences (expressed in F-values) between present and absent phosphenes. Right TMS data were flipped so that stimulation sites overlapped. X and Y axes represent, respectively, time in milliseconds and electrodes (from posterior to anterior ones). The two lines superimposed represent the GMFPs associated with the two conditions, whose peaks were used to identify TEPs clusters. The vertical dotted lines highlight GMFP peaks. The scalp topographies represent scalp differences between the two conditions ("Phosphene present" – "Phosphene absent"), with each map corresponding to the latency of each GMFP peak.

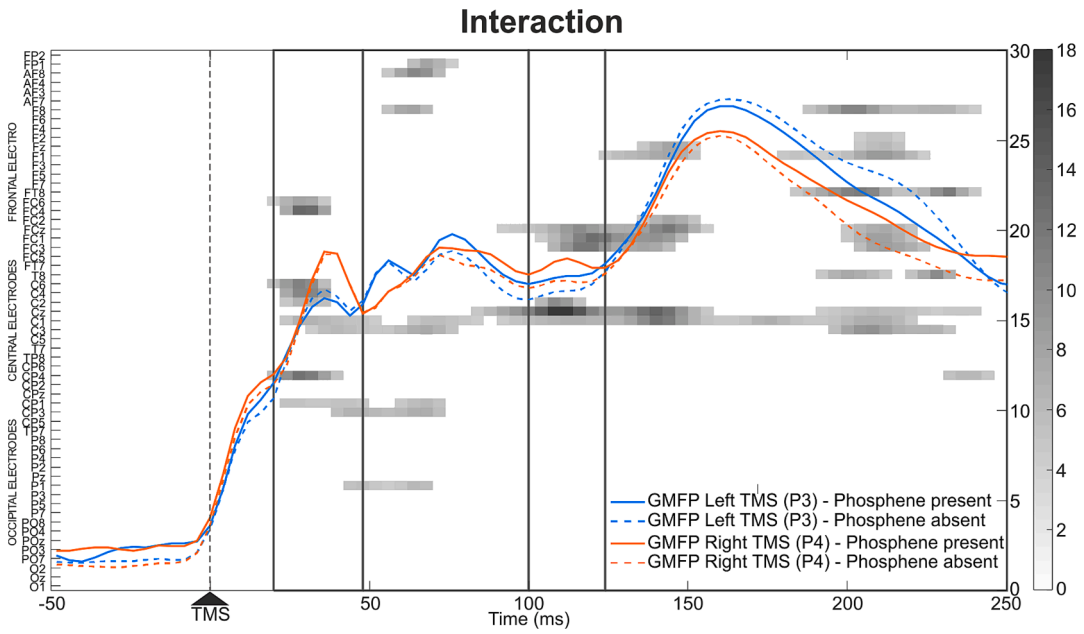

Fig. 6. Results from the ANOVA conducted on TEPs: interaction between *Stimulation site* and *Phosphene awareness*. Raster plot depicting for each time point and each electrode the significant differences (expressed in F-values) between the four different conditions ("Left TMS-Phosphene present"; "Left TMS-Phosphene absent"; "Right TMS-Phosphene present"; "Right TMS-Phosphene absent"). X and Y axes, respectively, represent time in milliseconds and electrodes (from posterior to anterior ones). The four lines superimposed represent the GMFPs associated with the four conditions, whose peaks were used to identify TEP clusters.

electrodes; source analysis revealed the generator of this component to be in BA 6, in the superior frontal gyrus (MNI coordinates: X= 10; Y= 5; Z= 70). The second component consisted of a negative pole located centrally, with smaller positive dipoles over parieto-occipital electrodes; source analysis revealed its origin to be in BA 7, in the postcentral gyrus (MNI coordinates: X= -20; Y= -55; Z= 70). The third component presented a topography displaying a negativity over parieto-central electrodes, engaging both sides of the scalp; source analysis revealed an origin located in BA 7, in the precuneus (MNI coordinates: X= 5; Y= -65; Z= 65). The fourth component showed a dipole with positivity over occipital and parietal electrodes and negativity over contralateral temporal electrodes; source analysis showed that this component originated in BA7, in the superior parietal lobule (MNI coordinates: X= -15; Y= -55; Z= 60). The fifth component displayed a topography characterized by a positive activation over centro-parietal electrodes, mainly leaning towards the ipsilateral hemisphere; source analysis showed that this component originates in BA 7, in the postcentral gyrus (MNI coordinates: X= 25; Y= -55; Z= 70).

Backprojecting the components on data averaged across the four different conditions revealed significant differences [all ps < 0.05, FDR corrected] for the *Stimulation site* condition in the first component: the two stimulated sites differ in the time windows 12-20 ms, 28-36 ms, 68-132 ms and 244-250 ms. Significant differences for the *Stimulation site* were also detected in the second component, lasting for the entire epoch duration, from 12 to 250 ms. The fourth component, on the other hand, showed significant differences for *Phosphene awareness*: the two conditions are significantly different from 40 to 60 ms (Fig. 9, right).

4. Discussion

In the last decades, the initial discovery of IPS as an independent phosphene generator (Bagattini et al., 2015; Knight et al., 2024; Marzi et al., 2009; Mazzi et al., 2014, 2017a; Parks et al., 2015; Tapia et al., 2014) has received progressive support. However, many aspects remain to be clarified, one of them being the existence of lateralized differences between the two IPS in the electrophysiological activity sustaining phosphenes. With the present study, therefore, we aimed to investigate the presence of hemispheric differences in IPS, specifically in the neural mechanisms associated with generating phosphenes.

To do so, we performed a TMS-EEG experiment stimulating both IPS at PT intensity so that we could directly compare the EEG activity elicited by phosphene perception across the two stimulated sites: this allowed us to reveal hemispheric asymmetries in the electrophysiological dynamics related to phosphene perception.

RTs for the "phosphene present" condition were significantly slower than RTs for the "phosphene absent" condition, in general contrast with previous research providing evidence of faster RTs for the "phosphene present" than for the "phosphene absent" condition – for both occipital and parietal (Bonfanti et al., 2024; Knight et al., 2024). However, caution must be assumed when making these comparisons. In fact, we did not emphasize to participants that they should answer as fast as they could; instead, they answered when they were sure about their response. This, in conjunction with the fact that parietal phosphenes are less vivid and bright than occipital ones (Mazzi et al., 2014) – also determined by the fact that our stimulations were below threshold – might explain why our participants needed a longer interval to report the presence of a phosphene: given the faint aspect of parietal phosphenes, they needed more time to be sure that they had actually perceived one, thus resulting in a longer interval for "phosphene present" condition.

To analyze our TMS-evoked data, we employed three different approaches. The first one is based on LMFP, giving us an overview of the general state of activation of the cortex. The second focuses on analyzing TMS-evoked potential through a hierarchical linear model: this allows us to statistically test all the time points and electrodes of EEG data, going beyond traditional approaches based on choosing specific mean amplitudes or wave peaks. Finally, correlated component analysis (CorrCA) is a source separation model that identifies source signals that are reliably reproduced across subjects. In this way, CorrCA goes beyond the sensor level, separating and displaying the sources of the brain activity recorded at the scalp level and providing, therefore, an electrophysiological rationale for the evoked neural activations analyzed with the previous approaches.

The LMFP is a time-domain, reference-free metric linked with TEPs. It represents the standard deviation of EEG activity caused by an event (in this case, a TMS pulse) in a cluster of electrodes of choice. This measure quantifies, therefore, the electrical response of the brain at each

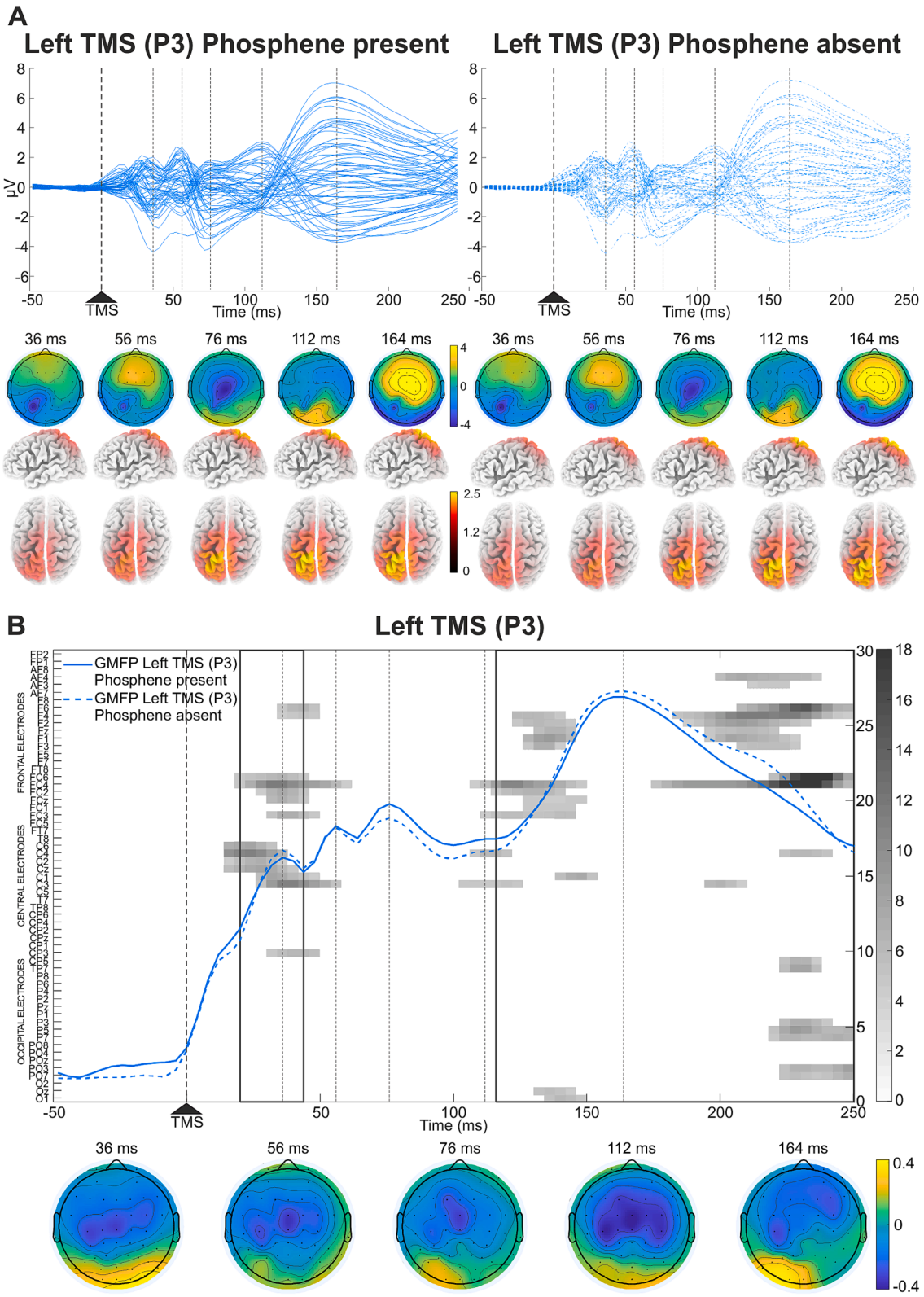

Fig. 7. Results from the ANOVA conducted on TEPs: post hoc pairwise comparison between "Phosphene present" and "Phosphene absent" for left TMS. A: Butterfly plots depicting TEPs for the two conditions ("Phosphene present", continuous line; "Phosphene absent", dotted line). Vertical dotted lines highlight the peaks of the different components, as determined by GMFP below. The topographies below represent the scalp distribution for each component, with corresponding source reconstruction. B: Raster plot depicting for each time point and each electrode the significant differences (expressed in F-values) between present and absent phosphenes. X and Y axes represent, respectively, time in milliseconds and electrodes (from posterior to anterior ones). The two lines superimposed represent the GMFPs associated with the two conditions, whose peaks were used to identify TEPs clusters. The vertical dotted lines highlight GMFP peaks. The scalp topographies represent scalp differences between the two conditions ("Phosphene present" – "Phosphene absent"), with each map corresponding to the latency of each GMFP peak.

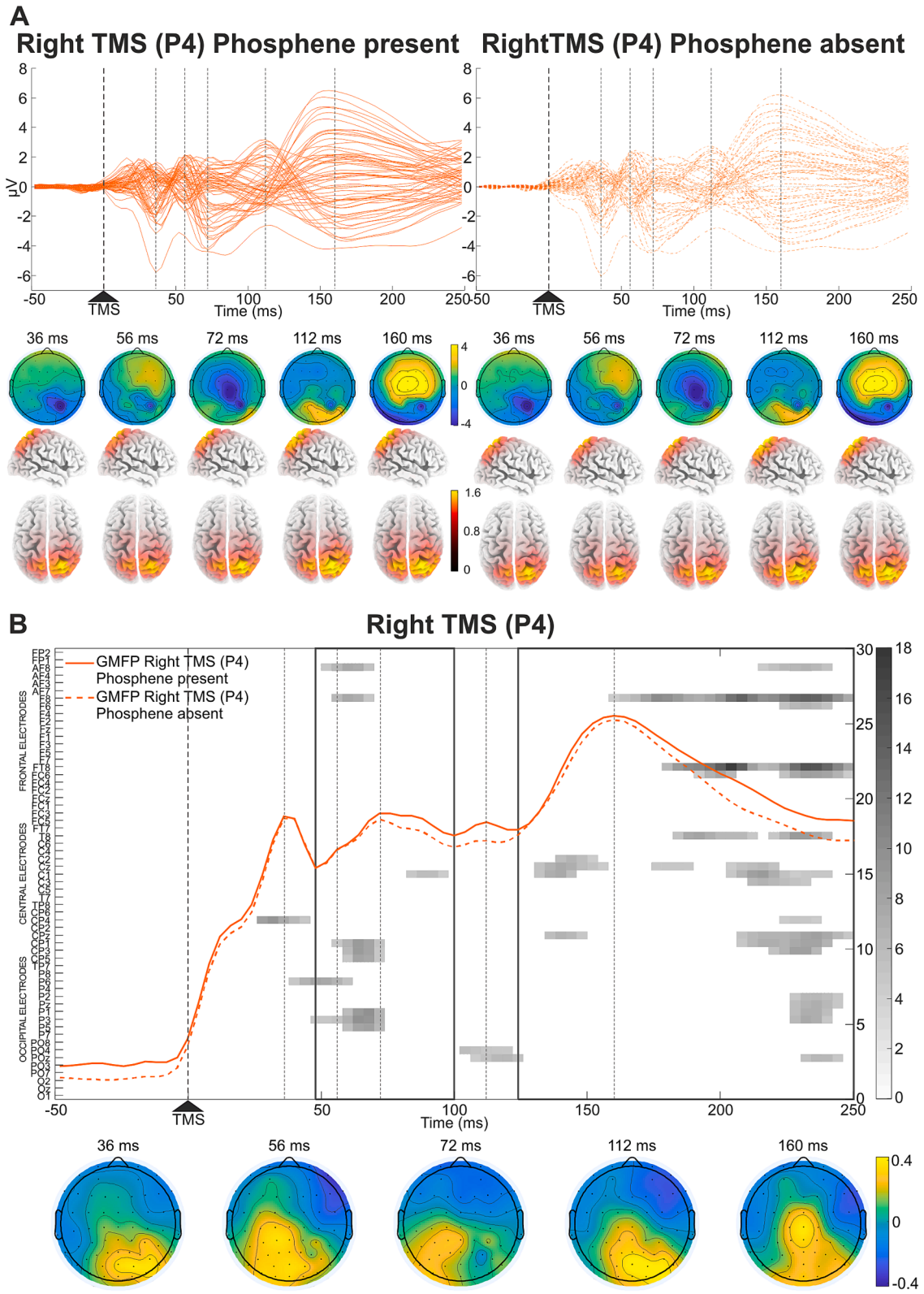

Fig. 8. Results from the ANOVA conducted on TEPs: post hoc pairwise comparison between "Phosphene present" and "Phosphene absent" for right TMS. A: Butterfly plots depicting TEPs for the two conditions ("Phosphene present", continuous line; "Phosphene absent", dotted line). Vertical dotted lines highlight the peaks of the different components, as determined by GMFP below. The topographies below represent the scalp distribution for each component, with corresponding source reconstruction. B: Raster plot depicting for each time point and each electrode the significant differences (expressed in F-values) between present and absent phosphenes. X and Y axes represent, respectively, time in milliseconds and electrodes (from posterior to anterior ones). The two lines superimposed represent the GMFPs associated with the two conditions, whose peaks were used to identify TEPs clusters. The vertical dotted lines highlight GMFP peaks. The scalp topographies represent scalp differences between the two conditions ("Phosphene present" – "Phosphene absent"), with each map corresponding to the latency of each GMFP peak.

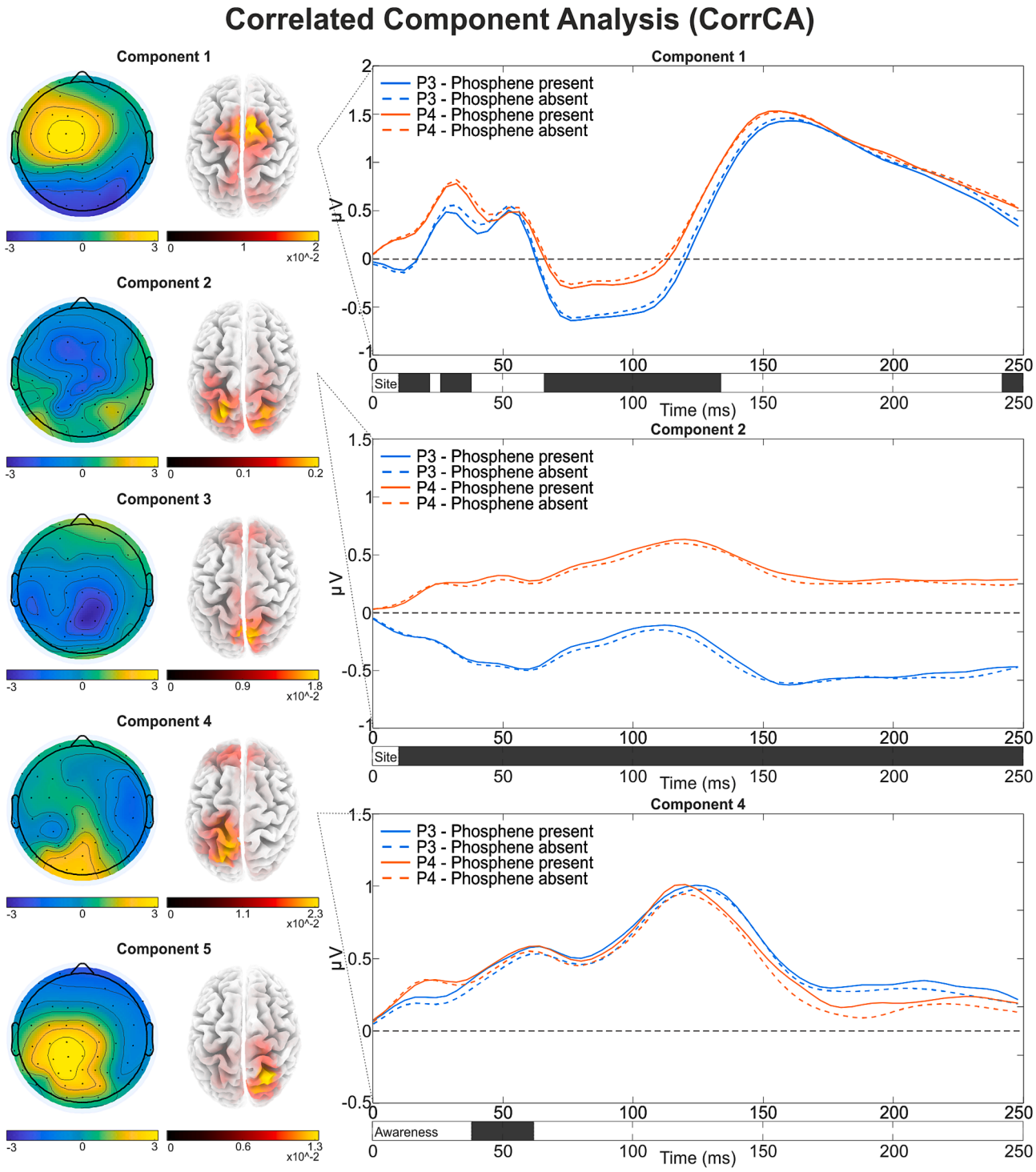

Fig. 9. CorrCA results. Left: topographies of the five significant components detected by CorrCA, with the respective source reconstructions. Right: backprojections of components 1, 2, and 4 – the ones showing an effect of either *Stimulation site* or *Phosphene awareness* – on the four conditions separately.

time point in the considered electrodes, providing an easily understandable and straightforward measure of local cortical activation following a specific event (Casarotto et al., 2013; Cruciani et al., 2023; Rocchi et al., 2018). We decided to calculate a "hemispheric" LMFP, clustering together the electrodes located on each side of the scalp (with the exclusion of the midline) to have an overview of the overall level of activation of right and left channels. Our data revealed a significant effect of the side of stimulation: electrodes ipsilateral to the stimulation showed a significantly higher activation level from 12 ms – i.e., from the first time point we started considering after the interpolation – to 100 ms compared to electrodes contralateral to the stimulation. This result shows, on one side, the efficacy of our TMS stimulation, proving that the level of activity in the stimulated half of the scalp is significantly higher than that of the non-stimulated half of the scalp. Moreover, it gives us an overview of the spread of TMS-induced activity across channels: LMFP points to the existence of an early time window – from stimulation up to 100 ms – during which the elicited activity remains confined to ipsilateral channels, and a later time window, during which the elicited signal becomes more homogeneous across the scalp, and the differences in terms of the level of activation between the two sides disappear. Other

studies have identified activity in the first 80-100 ms as reflecting genuine local cortical responses to TMS (Casula et al., 2022; Herring et al., 2015; Rocchi et al., 2021), possibly due to trans-synaptical connectivity mainly mediated by GABAergic interneurons (Premoli et al., 2014). However, the fact that in our LMFP analyses these early differences (e.g., <100 ms) in cortical activation were present for the whole time interval, not just when considering the electrodes surrounding the stimulation but also when considering an entire side of the scalp, raises some questions about the topographical extension of this so-called "local" response (i.e., how local it actually is) and the neurosynaptic mechanisms involved. A similar study targeting occipital areas found similar results in this regard (Bonfanti et al., 2024), further stressing the need for better elucidation of the mechanisms underlying the spread of TMS across neurons.

To our knowledge, our study is the first to directly compare TEPs deriving from phosphenes perception elicited by IPS stimulation of both hemispheres in a cohort of healthy participants. Previous TMS-EEG studies investigating parietal phosphenes have either investigated hemianopic patients (Mazzi et al., 2017a) or have focused on only one hemisphere (Bagattini et al., 2015; Samaha et al., 2017). Moreover, our analysis was not restricted to electrodes and time windows arbitrarily chosen but instead took into account the whole epoch and scalp coverage, allowing us to have a deeper understanding of TMS-induced activity across the brain (Bonfanti et al., 2024).

Looking at the effect of the stimulated site on the elicited brain response, we found that left and right IPS stimulation display a different pattern of activations: they first start to differ as soon as ~40 ms, with the most differences located at 50-70 ms and 150-250 ms. Source reconstruction revealed a different activation spread, with left IPS eliciting a larger activation diffusing centro-frontally towards the anterior part of the brain; on the other hand, right IPS determined a more restricted activation focused on centro-parietal areas. Ultimately, these differences might be due to the specialization of the right hemisphere for visual processing (Koch et al., 2011; Pisella et al., 2011; Roser et al., 2011), which could affect the degree of involvement of the stimulated areas: less specialized areas – in our case, left IPS – require a major cortical contribution from the surrounding cortex with respect to the more specialized in a specific function, in a way that is similar to the effect of a brain injury on the localization of function, which often results in this function necessitating a wider cortical contribution when the default area is deactivated by the injury (Grefkes et al., 2020; Rossini et al., 2003). With regard to the effect of phosphene perception on the elicited EEG activity, the most consistent differences appear to be during the time windows 100-150 ms and after 200 ms. Source reconstruction noticeably reveals that, for the entire epoch, the focus of this activity is centered on IPS, even for the activity associated with the "phosphene present" condition: this further proves the independence of IPS as a phosphene generator (Bagattini et al., 2015; Fried et al., 2011; Knight et al., 2024; Marzi et al., 2009; Mazzi et al., 2014, 2017a, 2019; Parks et al., 2015; Samaha et al., 2017; Tapia et al., 2014), with no activations in occipital areas that might be responsible for these percepts. Moreover, differences between the "phosphene present" and "phosphene absent" conditions seem to rely mainly on different degrees of activation of the stimulated area, rather than on different areas activated in the two conditions (Knight et al., 2024).

We then disentangled the effect of phosphene perception in the two stimulated sites. After left IPS TMS, phosphene perception elicited differential activations starting from ~30 ms, mainly present over central and frontal electrodes. The following activation is between 120 ms and 250 ms, involving frontal, central, and parieto-occipital electrodes. Source reconstruction shows that cortical activations spread mainly around IPS, again with no involvement of the occipital lobe, moving towards central and frontal areas as the epoch goes on. In a TMS-EEG study targeting left IPS to elicit phosphenes, Bagattini and colleagues (Bagattini et al., 2015) showed that the earliest onset latency of phosphenes awareness was at 66 ms, ~30 ms later than the activation we found; this difference is due to the fact that Bagattini and colleagues started analyzing TEPs from 50 ms, therefore missing out on everything that happened immediately after the stimulation. The later fronto-central and centro-parietal activations that they report in their study, on the other side, are partially in accordance with the second cluster of differential activations we found, confirming the existence of this second wave of frontal and posterior activity related to phosphene perception. In another TMS-EROS investigation of parietal phosphenes, Knight and colleagues (Knight et al., 2024) report that phosphene-related activity is initially limited to the stimulated IPS, in a time window ranging from ~50 to ~75 ms, again slightly later than the one we found. They also found later activations related to phosphene perception in the ~140-220 ms time window, which mainly involve occipital areas; this is in sharp contrast with our source reconstruction results, showing that stimulation activity remains constrained to the parietal lobe. Considering that previous research has demonstrated that IPS stimulation can elicit phosphenes even in patients who have undergone complete destruction of primary visual areas (Corbetta et al., 2008; Culham & Valyear, 2006; Xu G.Q. et al., 2016), it seems plausible to consider those late occipital activations as neural *consequences* of consciousness and not *proper correlates* of it (de Graaf et al., 2012).

With regards to phosphene perception after right IPS stimulation, we report a first differential activation between 60 and 70 ms, mainly involving parietal and centro-parietal electrodes. The following activation involves electrodes scattered across the scalp, including frontal, central, and parietal, in a time range starting at 150 ms and ending at 250 ms. Source reconstruction also shows for right IPS that phosphene-related activity spreads primarily around the stimulated site, with again no involvement of occipital areas, further confirming even right IPS as an independent phosphene generator. Differently from left IPS stimulation, however, right sources are more spread on posterior areas, with lesser involvement of the frontal lobe and major activations in parietal regions. Additionally, these activations are more centered around the stimulated point than their counterparts after left stimulation: phosphene-related activity confined to parietal areas can again reflect the more specialized nature of the right hemisphere for processing visual information and, therefore, less widespread recruitment of neuronal populations than the less visually specialized left hemisphere (Grefkes et al., 2020; Koch et al., 2011; Pisella et al., 2011; Roser et al., 2011; Rossini et al., 2003).

In a TMS-EEG study conducted on a hemianopic patient, Mazzi and colleagues (Mazzi et al., 2017a) report, for right parietal stimulation, that phosphene perception elicited significantly different activity from ~50 ms to ~80 ms, specifically at parieto-occipital and central electrodes. This matches the differential activations we found in our first cluster, involving mostly parietal and central electrodes.

Overall, our TEP analysis reveals that the first activations related to phosphene perception differ between the two stimulated sites both in terms of latency and spread. The second activation, on the other side, presents similar latency but different topographical characteristics. These diverse patterns of activation sustain the existence of lateralized differences between the two hemispheres in the electrophysiological mechanisms responsible for visual percepts. It is noteworthy, however, that participants did not report – although at an anecdotal level – any qualitative difference between right and left phosphenes.

To further analyze our results, we have used CorrCA (Dmochowski et al., 2012; Parra et al., 2018). CorrCA is a source separation technique that extracts linear components that are most reliable across subjects – i.e., that are maximally correlated when confronting two different time series. This process reduces data characterized by high-dimensionality (such as EEG) to just a few components, explaining activity common across different experimental conditions. Similarly to other blind source separation models (e.g., ICA, PCA), CorrCA allows a more thorough comprehension of TMS-related brain dynamics than observation of scalp channels since the effects of source (and potentially artifacts) mixing due to volume conduction can be strongly diminished – as long as they are

not shared across subjects. The comparison of the found components allowed us to ascertain how shared activity is modulated by the different experimental conditions, and where the sources of these modulations are located. To our knowledge, this technique has been applied only once on TMS-EEG data (D'Ambrosio et al., 2022), with the aim of extracting shared components. In this work, instead, we compared extracted components across different conditions, further characterizing the neural activity deriving from the two stimulated sites and the perception of phosphenes. Our analysis found five different correlated components. Of these five, the first and the second showed an effect of site of stimulation, while the fourth showed an effect of phosphene awareness.

Source reconstruction of the first component reveals that it mainly involves areas located along the midline, from parietal to motor areas; this might relate to differences in the diffusion of the neural signal, with activity from left IPS stimulation diffusing more frontally and activity from right IPS more posteriorly, with possibly a different involvement of the corpus callosum in the two conditions (Marzi et al., 1991; Marzi et al., 2009). It is known, in fact, that TMS on parietal areas surrounding IPS can exert interhemispheric influences (Heinen et al., 2011), affecting remote brain areas via callosal connections. The difference we report could be due to architectural differences supporting how the signal propagates after originating in the two stimulated sites.

The second component, too, shows an effect of the stimulated site, this time more posterior and centered on the stimulated IPS and its contralateral homologous. The differential activation on stimulated IPS could reflect differences in how the two IPS respond to TMS, as also reflected in our TEP results: a more localized activation following stimulation of right IPS, more specialized in visuospatial processing, and a more widespread activation following stimulation of left IPS, less specialized in visuospatial processing and therefore in need of recruiting a more comprehensive network when stimulated. In fact, it is known that the right hemisphere – and right parietal areas in particular – has a predominant role in processing visuospatial information (Marshall & Fink, 2001; Sack, 2009; Ten Brink et al., 2016), and the difference we found for this component might reflect differences in how IPS neurons – likely involved in visuospatial processing – process incoming stimuli. On the other hand, differences in IPS contralateral to stimulation might again be due to differences in the subcortical structures connecting the two IPS, resulting in differential activations between the two sites (Marzi et al., 2009).

The fourth detected component shows an effect of phosphene awareness at an early time window, ranging from 40 to 60 ms. Source reconstruction reveals that this differential activation is consistent with a localization over stimulated IPS. This is in accordance with our TEP results, as the activity related to phosphene perception in both left and right IPS shares the latency – particularly of the first cluster of electrodes – and source distribution of our CorrCA results. Moreover, these latter results further display that IPS can be a phosphene generator independent of occipital areas (Bagattini et al., 2015; Fried et al., 2011; Knight et al., 2024; Marzi et al., 2009; Mazzi et al., 2014, 2017a, 2019; Parks et al., 2015; Samaha et al., 2017; Tapia et al., 2014), further confirming that areas located along the dorsal stream – as IPS – can elicit conscious visual percepts and potentially play a role in visual awareness.

A similar investigation has been conducted by Bonfanti and colleagues (Bonfanti et al., 2024), using a comparable experimental paradigm to study the lateralization of early visual cortex responses to phosphene perception. What they found is the existence of lateralized differences in phosphene-related activity. They report that right and left TMS-evoked phosphenes elicit differential patterns of electrophysiological responses. Moreover, they also detected lateralized differences in how the signal propagates: while TMS on the right early visual cortex elicited early stronger activations and diffused more ipsilaterally, TMS on the left early visual cortex determined later stronger activations, spreading mainly contralaterally. These differences were further corroborated through connectivity analysis by another study conducted on the same dataset (Siviero et al., 2023). Overall, these papers support the existence of lateralized differences in the electrophysiological correlates of phosphenes, either occipital or parietal; moreover, they suggest that the two hemispheres can give rise to equivalent visual percepts despite them having different neural correlates and that this holds across different visually-responsive areas.

Despite the accumulating evidence demonstrating the existence of parietal phosphenes as a separate phenomenon from occipital phosphenes, with their reliability proved across different experiments and laboratories, some concern about the actual origin of parietal phosphenes still persists. As an example, Webster and Ro (Webster & Ro, 2017) showed that also TMS of the vertex could elicit phosphenes and that the probability of reporting them was inversely related to head size, suggesting the early visual cortex as their generator since the distance between the coil and the occipital lobe is smaller for smaller heads. In this paper, the authors use these results to question the origin of parietal phosphenes, suggesting that they might be generated by current spread or orthodromic/antidromic stimulation. Nevertheless, these results present several problems that need to be addressed. Firstly, the authors suggest that vertex phosphenes are generated in early visual areas thanks to TMS indirectly stimulating the occipital lobe, as proven by the inverse correlation with head size. However, this argument could hold even better assuming a parietal origin for these phosphenes: as IPS is closer to the vertex than the early visual cortex, indirect currents could even more easily stimulate parietal areas and elicit in this way parietal phosphenes. Secondly, Webster and Ro fail to find a correlation between TMS intensity and perception of vertex phosphenes, going against a wealth of literature showing a direct correlation between the strength of the TMS pulse and the probability of perceiving a phosphene, either occipital or parietal (Gerwig et al., 2003; Kammer et al., 2005; Kammer & Baumann, 2010; Mazzi et al., 2014; Salminen-Vaparanta et al., 2014). Finally, while the authors comment that vertex and occipital phosphenes' descriptions were "generally similar", it is also reported that 11 out of 18 participants reported differences in at least one aspect of these visual percepts, casting doubts on the possibility of a shared generator.

Our results could be read in the wake of the recent reconsideration of the two-streams hypothesis, based on the double dissociation between a ventral stream, seen as responsible for visual identification of objects, and a dorsal one, thought to be in charge of visuomotor guidance of action. In the last years, a series of studies has started questioning this model, often claiming that the proposed distinction is excessively sharp to account for the actual behavior of these two processing streams. Freud and colleagues, in a review investigating the role of the dorsal stream in visual perception (Freud et al., 2016), report that dorsal areas are capable of object representations that are independent of motor execution or planning. Specifically, they report the existence of object representations in the posterior dorsal pathway (corresponding to IPS) that are insensitive to image transformations, even in a passive fixation task (Konen & Kastner, 2008) – a remarkable feature of these representations, considering that invariance is typically associated with ventral object representations and a necessary feature for object recognition. These representations seem to be distinct from ventral object representations: IPS, in fact, is known to have activation latencies to visual stimuli as early as peristriate occipital cortex (Regev et al., 2018) – possibly mediated by a fast subcortical magnocellular pathway (Wang W. et al., 2023): a result, this, also supported by similar latencies for phosphene perception between the present study and others (Bonfanti et al., 2024). Besides, IPS also exhibits specific properties that make it something more than a mere recipient of ventral activity – as being able to support object categorization independently from ventral areas (Ayzenberg & Behrmann, 2022b), with the dorsal stream capable of predicting the ventral response, rather than the other way around (Ayzenberg et al., 2023). Moreover, they might also have some functional relevance for behavioral tasks: lesion studies revealed that patients suffering from ventral damage still retained some degree of sensitivity to structural object representations (Freud et al., 2017; James

et al., 2003), as suggested by both behavioral performance and degree of activation of dorsal areas. Importantly, the reverse pattern is also true, with the perception of structural information being impaired by dorsal lesions (Vaina, 1989; Van Dromme et al., 2016). These results point to the existence of object representations in the dorsal stream that are independent of ventral ones, and that subserve a specific functional role in visual perception. More specifically, the dorsal stream might exhibit a representational gradient from perceptual to motor, with areas located closer and more connected to early visual areas (e.g., IPS) representing perceptual and visual properties of stimuli.

The present results, thus, could further support this change of perspective about the processing properties of the dorsal stream: as early visual areas are consistently linked with object perception, and targeting them with TMS elicits visual percepts in the form of phosphenes, in a similar way IPS, given its role in object perception, when stimulated via TMS gives a comparable perceptual output to that coming from early occipital areas, as these neurons engage in similar – although specific – tasks.

In a recent paper reconsidering this model (Ayzenberg & Behrmann, 2022a), Ayzenberg and Behrmann propose a more nuanced distinction between the dorsal and the ventral streams with regard to object recognition: the former, in fact, seems to compute global shape representations, which are forwarded to the ventral stream, more focused on local feature discrimination; here, the results of both computations support object recognition, combining the results of both ventral and dorsal processes (Ayzenberg & Behrmann, 2023a, 2023b).

While it is not straightforward to directly relate results from basic neurophysiological investigations on phosphenes with the study of higher-order functions such as object recognition, we think that our experiment might provide a straightforward example of the perceptual properties of the dorsal stream – particularly of left and right IPS – lending support to a reconsideration of the dorsal stream functions in visual perception.

With our study, we assess the different neural responses of left and right IPS to TMS, showing how both these areas can determine phosphenes and providing evidence of the hemispheric differences in the neural signature of parietal phosphenes. Future studies will have to better understand the actual role of IPS neurons involved in visuospatial processing, and build a bridge between their ability to elicit phosphenes and perceptually related functions.

Data availability statement

The data supporting the conclusions of this article are publicly available at: https://gin.g-node.org/DB_123/IPS_parietal_phosphenes

ORCID
Davide Bonfanti: https://orcid.org/0000-0001-7858-8244
Elena Bertacco: https://orcid.org/0009-0001-3267-2229
Chiara Mazzi: https://orcid.org/0000-0002-4966-9341
Silvia Savazzi: https://orcid.org/0000-0002-5333-9046

Declaration of competing interest

The authors declare that they have no known competing financial interests or personal relationships that could have appeared to influence the work reported in this paper.

Acknowledgements

D.B. Fondazione Cassa di Risparmio di Verona, Vicenza, Belluno e Ancona “Ricerca scientifica d’eccellenza 2018”, “Emergence of Consciousness: From neural dynamics to complex conscious behaviour” grant no. 2018.0861; C.M. was supported by MIUR D.M. 737/2021-“Neural correlates of perceptual awareness: from neural architecture to the preservation of conscious vision in brain tumor patients” and MIUR PRIN 2017, “From brain dynamics to restoration of visual awareness after damage to the visual cortex.’’ grant no. 2017TBA4KS_002; S.S. was supported by #NEXTGENERATIONEU (NGEU) and funded by the Ministry of University and Research (MUR), National Recovery and Resilience Plan (NRRP), project MNESYS (PE0000006) - “A Multiscale integrated approach to the study of the nervous system in health and disease” (DN. 1553 11.10.2022).

Appendix A. Supplementary data

Supplementary data to this article can be found online at https://doi.org/10.1016/j.clinph.2025.03.041.

References

Andersen, R.A., Cui, H., 2009. Intention, Action Planning, and Decision Making in Parietal-Frontal Circuits. *Neuron* 63 (5), 568–583. https://doi.org/10.1016/J.NEURON.2009.08.028.

Ayzenberg, V., & Behrmann, M. (2022a). Does the brain’s ventral visual pathway compute object shape? In *Trends in Cognitive Sciences* (Vol. 26, Issue 12, pp. 1119–1132). Elsevier Ltd. https://doi.org/10.1016/j.tics.2022.09.019.

Ayzenberg, V., Behrmann, M., 2022b. The Dorsal Visual Pathway Represents Object-Centered Spatial Relations for Object Recognition. *Journal of Neuroscience* 42 (23), 4693–4710. https://doi.org/10.1523/JNEUROSCI.2257-21.2022.

Ayzenberg, V., Behrmann, M., 2023a. An expanded neural framework for shape perception. *Trends in Cognitive Sciences* 27 (3), 212–213. https://doi.org/10.1016/J.TICS.2022.12.001.

Ayzenberg, V., Behrmann, M., 2023b. The where, what, and how of object recognition. *Trends in Cognitive Sciences* 27 (4), 335–336. https://doi.org/10.1016/j.tics.2023.01.006.

Ayzenberg, V., Simmons, C., Behrmann, M., 2023. Temporal asymmetries and interactions between dorsal and ventral visual pathways during object recognition. *Cerebral Cortex Communications* 4 (1), 1–12. https://doi.org/10.1093/TEXCOM/TGAD003.

Bagattini, C., Mazzi, C., Savazzi, S., 2015. Waves of awareness for occipital and parietal phosphenes perception. *Neuropsychologia* 70, 114–125. https://doi.org/10.1016/j.neuropsychologia.2015.02.021.

Ben-Shachar, M. S. (2020). *TBT: Reject and interpolate channels on a epoch by epoch basis*. https://doi.org/10.5281/ZENODO.3784278.

Bertazzoli, G., Esposito, R., Mutanen, T.P., Ferrari, C., Ilmoniemi, R.J., Miniussi, C., Bortoletto, M., 2021. The impact of artifact removal approaches on TMS–EEG signal. *NeuroImage* 239, 118272. https://doi.org/10.1016/J.NEUROIMAGE.2021.118272.

Bien, N., Goebel, R., Sack, A.T., 2012. Extinguishing Extinction: Hemispheric Differences in the Modulation of TMS-induced Visual Extinction by Directing Covert Spatial Attention. *Journal of Cognitive Neuroscience* 24 (4), 809–818. https://doi.org/10.1162/JOCN_A_00179.

Bonda, E., Petrides, M., Ostry, D., Evans, A., 1996. Specific Involvement of Human Parietal Systems and the Amygdala in the Perception of Biological Motion. *The Journal of Neuroscience* 76 (11), 3737–3744.

Bonfanti, D., Mazzi, C., Savazzi, S., 2024. Mapping the routes of perception: Hemispheric asymmetries in signal propagation dynamics. *Psychophysiology* 00, e14529. https://doi.org/10.1111/PSYP.14529.

Budisavljevic, S., Dell’Acqua, F., Zanatto, D., Begliomini, C., Miotto, D., Motta, R., Castiello, U., 2017. Asymmetry and Structure of the Fronto-Parietal Networks Underlie Visuomotor Processing in Humans. *Cerebral Cortex* 27 (2), 1532–1544. https://doi.org/10.1093/CERCOR/BHV348.

Capotosto, P., Babiloni, C., Romani, G.L., Corbetta, M., 2012. Differential contribution of right and left parietal cortex to the control of spatial attention: A simultaneous EEG-rTMS study. *Cerebral Cortex* 22 (2), 446–454. https://doi.org/10.1093/cercor/bhr127.

Casarotto, S., Canali, P., Rosanova, M., Pigorini, A., Fecchio, M., Mariotti, M., Lucca, A., Colombo, C., Benedetti, F., Massimini, M., 2013. Assessing the Effects of Electroconvulsive Therapy on Cortical Excitability by Means of Transcranial Magnetic Stimulation and Electroencephalography. *Brain Topography* 26 (2), 326. https://doi.org/10.1007/S10548-012-0256-8.

Casula, E. P., Leodori, G., Ibáñez, J., Benussi, A., Rawji, V., Tremblay, S., Latorre, A., Rothwell, J. C., & Rocchi, L. (2022). The Effect of Coil Orientation on the Stimulation of the Pre–Supplementary Motor Area: A Combined TMS and EEG Study. *Brain Sciences 2022, Vol. 12, Page 1358*, *12*(10), 1358. https://doi.org/10.3390/BRAINSCI12101358.

Colby, C. L., & Goldberg, M. E. (2003). SPACE AND ATTENTION IN PARIETAL CORTEX. *Https://Doi.Org/10.1146/Annurev.Neuro.22.1.319*, *22*, 319–349. https://doi.org/10.1146/ANNUREV.NEURO.22.1.319.

Corbetta, M., Patel, G., Shulman, G.L., 2008. The Reorienting System of the Human Brain: From Environment to Theory of Mind. *Neuron* 58 (3), 306–324. https://doi.org/10.1016/j.neuron.2008.04.017.

Corbetta, M., & Shulman, G. L. (2002). Control of goal-directed and stimulus-driven attention in the brain. *Nature Reviews Neuroscience 2002 3:3*, *3*(3), 201–215. https://doi.org/10.1038/nrn755.

Cruciani, A., Mancuso, M., Sveva, V., Maccarrone, D., Todisco, A., Motolese, F., Santoro, F., Pilato, F., Spampinato, D. A., Rocchi, L., Di Lazzaro, V., & Capone, F. (2023). Using TMS-EEG to assess the effects of neuromodulation techniques: a narrative

review. In *Frontiers in Human Neuroscience* (Vol. 17). Frontiers Media SA. https://doi.org/10.3389/fnhum.2023.1247104.
Culham, J.C., Valyear, K.F., 2006. Human parietal cortex in action. *Current Opinion in Neurobiology* 16 (2), 205–212. https://doi.org/10.1016/J.CONB.2006.03.005.
D'Ambrosio, S., Jiménez-Jiménez, D., Silvennoinen, K., Zagaglia, S., Perulli, M., Poole, J., Comolatti, R., Fecchio, M., Sisodiya, S.M., Balestrini, S., 2022. Physiological symmetry of transcranial magnetic stimulation-evoked EEG spectral features. *Human Brain Mapping* 43 (18), 5465–5477. https://doi.org/10.1002/HBM.26022.
de Graaf, T.A., Hsieh, P.J., Sack, A.T., 2012. The "correlates" in neural correlates of consciousness. In *Neuroscience and Biobehavioral Reviews* (Vol. 36 (1), 191–197. https://doi.org/10.1016/j.neubiorev.2011.05.012.
de Renzi, E.D., 1969. Perceptual and associative disorders of visual recognition: Relationship to the side of the cerebral lesion. *Neurology* 19 (7), 634–642. https://doi.org/10.1212/WNL.19.7.634/ASSET/CED7D56B-788F-40E8-9CCA-2C94FD9A7965/ASSETS/WNL.19.7.634.FP.PNG.
de Renzi, E., Spinnler, H., 1966. Visual recognition in patients with unilateral cerebral disease. *The Journal of Nervous and Mental Disease* 142 (6), 515–525. https://doi.org/10.1097/00005053-196606000-00002.
Delorme, A., Makeig, S., 2004. *EEGLAB : an open source toolbox for analysis of single-trial EEG dynamics including independent component analysis*. 134, 9–21. https://doi.org/10.1016/j.jneumeth.2003.10.009.
Delorme, A., Sejnowski, T., Makeig, S., 2007. Enhanced detection of artifacts in EEG data using higher-order statistics and independent component analysis. *NeuroImage* 34 (4), 1443–1449. https://doi.org/10.1016/J.NEUROIMAGE.2006.11.004.
Di Russo, F., Lucci, G., Sulpizio, V., Berchicci, M., Spinelli, D., Pitzalis, S., Galati, G., 2016. Spatiotemporal brain mapping during preparation, perception, and action. *NeuroImage* 126, 1–14. https://doi.org/10.1016/J.NEUROIMAGE.2015.11.036.
Dmochowski, J.P., Sajda, P., Dias, J., Parra, L.C., 2012. Correlated components of ongoing EEG point to emotionally laden attention - a possible marker of engagement? *Frontiers in Human Neuroscience*, *MAY* 2012. https://doi.org/10.3389/fnhum.2012.00112.
Dong, L., Li, F., Liu, Q., Wen, X., Lai, Y., Xu, P., Yao, D., 2017. MATLAB toolboxes for reference electrode standardization technique (REST) of scalp EEG. *Frontiers in Neuroscience* 11 (OCT), 601. https://doi.org/10.3389/fnins.2017.00601.
Duecker, F., Sack, A.T., 2015. The hybrid model of attentional control: New insights into hemispheric asymmetries inferred from TMS research. *Neuropsychologia* 74, 21–29. https://doi.org/10.1016/j.neuropsychologia.2014.11.023.
Ferro, J.M., Santos, M.E., 1984. Associative Visual Agnosia: A Case Study. *Cortex* 20 (1), 121–134. https://doi.org/10.1016/S0010-9452(84)80029-5.
Freud, E., Ganel, T., Shelef, I., Hammer, M.D., Avidan, G., Behrmann, M., 2017. Three-Dimensional Representations of Objects in Dorsal Cortex are Dissociable from Those in Ventral Cortex. *Cerebral Cortex* 27 (1), 422–434. https://doi.org/10.1093/CERCOR/BHV229.
Freud, E., Plaut, D. C., & Behrmann, M. (2016). 'What' Is Happening in the Dorsal Visual Pathway. In *Trends in Cognitive Sciences* (Vol. 20, Issue 10, pp. 773–784). Elsevier Ltd. https://doi.org/10.1016/j.tics.2016.08.003.
Fried, P.J., Elkin-Frankston, S., Rushmore, R.J., Hilgetag, C.C., Valero-Cabre, A., 2011. Characterization of Visual Percepts Evoked by Noninvasive Stimulation of the Human Posterior Parietal Cortex. *PLOS ONE* 6 (11), e27204. https://doi.org/10.1371/JOURNAL.PONE.0027204.
Fuchs, M., Kastner, J., Wagner, M., Hawes, S., Ebersole, J.S., 2002. A standardized boundary element method volume conductor model. *Clinical Neurophysiology* 113 (5), 702–712. https://doi.org/10.1016/S1388-2457(02)00030-5.
Fulvio, J.M., Haegens, S., Postle, B.R., 2024. Single-pulse Transcranial Magnetic Stimulation Affects Working-memory Performance via Posterior Beta-band Oscillations. *Journal of Cognitive Neuroscience* 36 (9), 1827–1846. https://doi.org/10.1162/JOCN_A_02194.
Gerwig, M., Kastrup, O., Meyer, B.U., Niehaus, L., 2003. Evaluation of cortical excitability by motor and phosphene thresholds in transcranial magnetic stimulation. *Journal of the Neurological Sciences* 215 (1–2), 75–78. https://doi.org/10.1016/S0022-510X(03)00228-4.
Goodale, M.A., Milner, A.D., 1992. Separate visual pathways for perception and action. *Trends in Neurosciences* 15 (1), 20–25. https://doi.org/10.1016/0166-2236(92)90344-8.
Grech, R., Cassar, T., Muscat, J., Camilleri, K.P., Fabri, S.G., Zervakis, M., Xanthopoulos, P., Sakkalis, V., Vanrumste, B., 2008. Review on solving the inverse problem in EEG source analysis. *Journal of NeuroEngineering and Rehabilitation* 5 (1), 1–33. https://doi.org/10.1186/1743-0003-5-25/COMMENTS.
Grefkes, C., Grefkes, C., Fink, G.R., Fink, G.R., 2020. Recovery from stroke: Current concepts and future perspectives. *Neurological Research and Practice* 2 (1), 1–10. https://doi.org/10.1186/S42466-020-00060-6/FIGURES/4.
Groppe, D.M., Urbach, T.P., Kutas, M., 2011. Mass univariate analysis of event-related brain potentials/fields I: A critical tutorial review. *Psychophysiology* 48 (12), 1711–1725. https://doi.org/10.1111/J.1469-8986.2011.01273.X.
Heinen, K., Ruff, C.C., Bjoertomt, O., Schenkluhn, B., Bestmann, S., Blankenburg, F., Driver, J., Chambers, C.D., 2011. Concurrent TMS-fMRI reveals dynamic interhemispheric influences of the right parietal cortex during exogenously cued visuospatial attention. *European Journal of Neuroscience* 33 (5), 991–1000. https://doi.org/10.1111/j.1460-9568.2010.07580.x.
Herring, J.D., Thut, G., Jensen, O., Bergmann, T.O., 2015. Attention Modulates TMS-Locked Alpha Oscillations in the Visual Cortex. *Journal of Neuroscience* 35 (43), 14435–14447. https://doi.org/10.1523/JNEUROSCI.1833-15.2015.
Husain, M., Nachev, P., 2007. Space and the parietal cortex. *Trends in Cognitive Sciences* 11 (1), 30–36. https://doi.org/10.1016/J.TICS.2006.10.011.
James, T.W., Culham, J., Humphrey, G.K., Milner, A.D., Goodale, M.A., 2003. Ventral occipital lesions impair object recognition but not object-directed grasping: An fMRI study. *Brain* 126 (11), 2463–2475. https://doi.org/10.1093/brain/awg248.
JASP Team. (2020). *JASP* (0.13.1).
Jatoi, M.A., Kamel, N., Malik, A.S., Faye, I., 2014. EEG based brain source localization comparison of sLORETA and eLORETA. *Australasian Physical & Engineering Sciences in Medicine* 37 (4), 713–721. https://doi.org/10.1007/S13246-014-0308-3.
Jeong, S.K., Xu, Y., 2016. *Behaviorally Relevant Abstract Object Identity Representation in the Human Parietal Cortex*. https://doi.org/10.1523/JNEUROSCI.1016-15.2016.
Jurcak, V., Tsuzuki, D., Dan, I., 2007. 10/20, 10/10, and 10/5 systems revisited: their validity as relative head-surface-based positioning systems. *NeuroImage* 34 (4), 1600–1611. https://doi.org/10.1016/J.NEUROIMAGE.2006.09.024.
Kammer, T., Baumann, L.W., 2010. Phosphene thresholds evoked with single and double TMS pulses. *Clinical Neurophysiology* 121 (3), 376–379. https://doi.org/10.1016/J.CLINPH.2009.12.002.
Kammer, T., Puls, K., Erb, M., Grodd, W., 2005. Transcranial magnetic stimulation in the visual system. II. Characterization of induced phosphenes and scotomas. *Experimental Brain Research* 160 (1), 129–140. https://doi.org/10.1007/s00221-004-1992-0.
Kinsbourne, M., 1977. Hemi-neglect and hemisphere rivalry. *Advances in Neurology* 18, 41–49.
Knight, R.S., Chen, T., Center, E.G., Gratton, G., Fabiani, M., Savazzi, S., Mazzi, C., Beck, D.M., 2024. Bypassing input to V1 in visual awareness: A TMS-EROS investigation. *Neuropsychologia* 198, 108864. https://doi.org/10.1016/J.NEUROPSYCHOLOGIA.2024.108864.
Koch, G., Cercignani, M., Bonnì, S., Giacobbe, V., Bucchi, G., Versace, V., Caltagirone, C., Bozzali, M., 2011. Asymmetry of parietal interhemispheric connections in humans. *Journal of Neuroscience* 31 (24), 8967–8975. https://doi.org/10.1523/JNEUROSCI.6567-10.2011.
Konen, C. S., & Kastner, S. (2008b). Two hierarchically organized neural systems for object information in human visual cortex. *Nature Neuroscience 2008 11:2*, *11*(2), 224–231. https://doi.org/10.1038/nn2036.
Kravitz, D. J., Saleem, K. S., Baker, C. I., & Mishkin, M. (2011). A new neural framework for visuospatial processing. *Nature Reviews Neuroscience 2011 12:4*, *12*(4), 217–230. https://doi.org/10.1038/nrn3008.
Lehmann, D., Skrandies, W., 1980. Reference-free identification of components of checkerboard-evoked multichannel potential fields. *Electroencephalography and Clinical Neurophysiology* 48 (6), 609–621. https://doi.org/10.1016/0013-4694(80)90419-8.
Marshall, J.C., Fink, G.R., 2001. Spatial cognition: Where we were and where we are. *NeuroImage* 14 (1 II). https://doi.org/10.1006/nimg.2001.0834.
Marzi, C.A., Bisiacchi, P., Nicoletti, R., 1991. Is interhemispheric transfer of visuomotor information asymmetric? Evidence from a meta-analysis. *Neuropsychologia* 29 (12), 1163–1177. https://doi.org/10.1016/0028-3932(91)90031-3.
Marzi, C.A., Mancini, F., Savazzi, S., 2009. Interhemispheric transfer of phosphenes generated by occipital versus parietal transcranial magnetic stimulation. *Experimental Brain Research* 192 (3), 431–441. https://doi.org/10.1007/S00221-008-1496-4.
Mazzi, C., Mancini, F., Savazzi, S., 2014. Can IPS reach visual awareness without V1? Evidence from TMS in healthy subjects and hemianopic patients. *Neuropsychologia* 64, 134–144. https://doi.org/10.1016/j.neuropsychologia.2014.09.026.
Mazzi, C., Mazzeo, G., Savazzi, S., 2017b. Markers of TMS-evoked visual conscious experience in a patient with altitudinal hemianopia. *Consciousness and Cognition* 54, 143–154. https://doi.org/10.1016/j.concog.2017.01.022.
Mazzi, C., Savazzi, S., Abrahamyan, A., Ruzzoli, M., 2017a. Reliability of TMS phosphene threshold estimation: Toward a standardized protocol. *Brain Stimulation* 10 (3), 609–617. https://doi.org/10.1016/j.brs.2017.01.582.
Mazzi, C., Savazzi, S., Silvanto, J., 2019. On the "blindness" of blindsight: What is the evidence for phenomenal awareness in the absence of primary visual cortex (V1)? *Neuropsychologia* 128, 103–108. https://doi.org/10.1016/j.neuropsychologia.2017.10.029.
Mazziotta, J., Toga, A., Evans, A., Fox, P., Lancaster, J., Zilles, K., Woods, R., Paus, T., Simpson, G., Pike, B., Holmes, C., Collins, L., Thompson, P., MacDonald, D., Iacoboni, M., Schormann, T., Amunts, K., Palomero-Gallagher, N., Geyer, S., … Mazoyer, B. (2001). A probabilistic atlas and reference system for the human brain: International Consortium for Brain Mapping (ICBM). *Philosophical Transactions of the Royal Society of London. Series B*, *356*(1412), 1293. https://doi.org/10.1098/RSTB.2001.0915.
Mutha, P.K., Sainburg, R.L., Haaland, K.Y., 2011. Left Parietal Regions Are Critical for Adaptive Visuomotor Control. *The Journal of Neuroscience* 31 (19), 6972. https://doi.org/10.1523/JNEUROSCI.6432-10.2011.
Parisi, G., Mazzi, C., Colombari, E., Chiarelli, A.M., Metzger, B.A., Marzi, C.A., Savazzi, S., 2020. Spatiotemporal dynamics of attentional orienting and reorienting revealed by fast optical imaging in occipital and parietal cortices. *NeuroImage* 222, 117244. https://doi.org/10.1016/J.NEUROIMAGE.2020.117244.
Parks, N.A., Mazzi, C., Tapia, E., Savazzi, S., Fabiani, M., Gratton, G., Beck, D.M., 2015. The influence of posterior parietal cortex on extrastriate visual activity: A concurrent TMS and fast optical imaging study. *Neuropsychologia* 78, 153–158. https://doi.org/10.1016/J.NEUROPSYCHOLOGIA.2015.10.002.
Parra, L. C., Haufe, S., & Dmochowski, J. P. (2018). *Correlated Components Analysis - Extracting Reliable Dimensions in Multivariate Data*. https://doi.org/10.51628/001c.7125.
Pascual-Marqui, R. D. (2007). Discrete, 3D distributed, linear imaging methods of electric neuronal activity. Part 1: exact, zero error localization. *ArXiv:0710.3341 [Math-Ph]*. http://arxiv.org/abs/0710.3341.

Pascual-Marqui, R.D., Lehmann, D., Koukkou, M., Kochi, K., Anderer, P., Saletu, B., Tanaka, H., Hirata, K., John, E.R., Prichep, L., Biscay-Lirio, R., Kinoshita, T., 2011. Assessing interactions in the brain with exact low-resolution electromagnetic tomography. *Philosophical Transactions. Series A, Mathematical, Physical, and Engineering Sciences* 369 (1952), 3768–3784. https://doi.org/10.1098/RSTA.2011.0081.

Pernet, C.R., Chauveau, N., Gaspar, C., Rousselet, G.A., 2011. LIMO EEG: A Toolbox for Hierarchical LInear MOdeling of ElectroEncephaloGraphic Data. *Computational Intelligence and Neuroscience* 2011, 11. https://doi.org/10.1155/2011/831409.

Pisella, L., Alahyane, N., Blangero, A., Thery, F., Blanc, S., Pelisson, D., 2011. Right-hemispheric dominance for visual remapping in humans. *Philosophical Transactions of the Royal Society B: Biological Sciences* 366 (1564), 572. https://doi.org/10.1098/RSTB.2010.0258.

Pisella, L., Binkofski, F., Lasek, K., Toni, I., Rossetti, Y., 2006. No double-dissociation between optic ataxia and visual agnosia: Multiple sub-streams for multiple visuo-manual integrations. *Neuropsychologia* 44 (13), 2734–2748. https://doi.org/10.1016/j.neuropsychologia.2006.03.027.

Premoli, I., Castellanos, N., Rivolta, D., Belardinelli, P., Bajo, R., Zipser, C., Espenhahn, S., Heidegger, T., Müller-Dahlhaus, F., Ziemann, U., 2014. *TMS-EEG Signatures of GABAergic Neurotransmission in the Human Cortex*. https://doi.org/10.1523/JNEUROSCI.5089-13.2014.

Radoeva, P.D., Cohen, J.D., Corballis, P.M., Lukovits, T.G., Koleva, S.G., 2005. Hemispheric asymmetry in a dissociation between the visuomotor and visuoperceptual streams. *Neuropsychologia* 43 (12), 1763–1773. https://doi.org/10.1016/J.NEUROPSYCHOLOGIA.2005.02.005.

Regev, T.I., Winawer, J., Gerber, E.M., Knight, R.T., Deouell, L.Y., 2018. Human posterior parietal cortex responds to visual stimuli as early as peristriate occipital cortex. *The European Journal of Neuroscience* 48 (12), 3567–3582. https://doi.org/10.1111/EJN.14164.

Rocchi, L., Di Santo, A., Brown, K., Ibáñez, J., Casula, E., Rawji, V., Di Lazzaro, V., Koch, G., Rothwell, J., 2021. Disentangling EEG responses to TMS due to cortical and peripheral activations. *Brain Stimulation* 14 (1), 4–18. https://doi.org/10.1016/J.BRS.2020.10.011.

Rocchi, L., Ibáñez, J., Benussi, A., Hannah, R., Rawji, V., Casula, E., Rothwell, J., 2018. Variability and predictors of response to continuous theta burst stimulation: A TMS-EEG study. *Frontiers in Neuroscience* 12 (JUN), 350969. https://doi.org/10.3389/FNINS.2018.00400/BIBTEX.

Rogasch, N. C., Sullivan, C., Thomson, R. H., Rose, N. S., Bailey, N. W., Fitzgerald, P. B., Farzan, F., & Hernandez-Pavon, J. C. (2017). Analysing concurrent transcranial magnetic stimulation and electroencephalographic data: A review and introduction to the open-source TESA software. *NeuroImage*, *147*(September 2016), 934–951. https://doi.org/10.1016/j.neuroimage.2016.10.031.

Rogasch, N.C., Thomson, R.H., Farzan, F., Fitzgibbon, B.M., Bailey, N.W., Hernandez-Pavon, J.C., Daskalakis, Z.J., Fitzgerald, P.B., 2014. Removing artefacts from TMS-EEG recordings using independent component analysis: Importance for assessing prefrontal and motor cortex network properties. *NeuroImage* 101, 425–439. https://doi.org/10.1016/J.NEUROIMAGE.2014.07.037.

Roser, M.E., Fiser, J., Aslin, R.N., Gazzaniga, M.S., 2011. Right hemisphere dominance in visual statistical learning. *Journal of Cognitive Neuroscience* 23 (5), 1088. https://doi.org/10.1162/JOCN.2010.21508.

Rossetti, Y., & Pisella, L. (2018). Optic ataxia: beyond the dorsal stream cliché. In *Handbook of Clinical Neurology* (Vol. 151, pp. 225–247). Elsevier B.V. https://doi.org/10.1016/B978-0-444-63622-5.00011-5.

Rossi, S., Hallett, M., Rossini, P. M., Pascual-Leone, A., Avanzini, G., Bestmann, S., Berardelli, A., Brewer, C., Canli, T., Cantello, R., Chen, R., Classen, J., Demitrack, M., Di Lazzaro, V., Epstein, C. M., George, M. S., Fregni, F., Ilmoniemi, R., Jalinous, R., … Ziemann, U. (2009). Safety, ethical considerations, and application guidelines for the use of transcranial magnetic stimulation in clinical practice and research. In *Clinical Neurophysiology* (Vol. 120, Issue 12, pp. 2008–2039). Elsevier. https://doi.org/10.1016/j.clinph.2009.08.016.

Rossini, P.M., Calautti, C., Pauri, F., Baron, J.C., 2003. Post-stroke plastic reorganisation in the adult brain. *The Lancet Neurology* 2 (8), 493–502. https://doi.org/10.1016/S1474-4422(03)00485-X.

Rushworth, M.F.S., Johansen-Berg, H., Göbel, S.M., Devlin, J.T., 2003. The left parietal and premotor cortices: motor attention and selection. *NeuroImage* 20 (SUPPL. 1), S89–S100. https://doi.org/10.1016/J.NEUROIMAGE.2003.09.011.

Sack, A.T., 2009. Parietal cortex and spatial cognition. *Behavioural Brain Research* 202 (2), 153–161. https://doi.org/10.1016/J.BBR.2009.03.012.

Salminen-Vaparanta, N., Vanni, S., Noreika, V., Valiulis, V., Móró, L., Revonsuo, A., 2014. Subjective Characteristics of TMS-Induced Phosphenes Originating in Human V1 and V2. *Cerebral Cortex* 24 (10), 2751–2760. https://doi.org/10.1093/CERCOR/BHT131.

Samaha, J., Gosseries, O., Postle, B.R., 2017. Distinct oscillatory frequencies underlie excitability of human occipital and parietal cortex. *Journal of Neuroscience* 37 (11), 2824–2833. https://doi.org/10.1523/JNEUROSCI.3413-16.2017.

Schluter, N.D., Krams, M., Rushworth, M.F.S., Passingham, R.E., 2001. Cerebral dominance for action in the human brain: the selection of actions. *Neuropsychologia* 39 (2), 105–113. https://doi.org/10.1016/S0028-3932(00)00105-6.

Silver, M.A., Kastner, S., 2009. Topographic maps in human frontal and parietal cortex. *Trends in Cognitive Sciences* 13 (11), 488–495. https://doi.org/10.1016/J.TICS.2009.08.005.

Siviero, I., Bonfanti, D., Menegaz, G., Savazzi, S., Mazzi, C., Storti, S.F., 2023. Graph Analysis of TMS–EEG Connectivity Reveals Hemispheric Differences following Occipital Stimulation. *Sensors* 23 (21), 8833. https://doi.org/10.3390/s23218833.

Sulpizio, V., Lucci, G., Berchicci, M., Galati, G., Pitzalis, S., Di Russo, F., 2017. Hemispheric asymmetries in the transition from action preparation to execution. *NeuroImage* 148, 390–402. https://doi.org/10.1016/J.NEUROIMAGE.2017.01.009.

Tapia, E., Mazzi, C., Savazzi, S., Beck, D.M., 2014. Phosphene-guided transcranial magnetic stimulation of occipital but not parietal cortex suppresses stimulus visibility. *Experimental Brain Research* 232 (6), 1989–1997. https://doi.org/10.1007/S00221-014-3888-Y.

Ten Brink, A.F., Matthijs Biesbroek, J., Kuijf, H.J., Van der Stigchel, S., Oort, Q., Visser-Meily, J.M.A., Nijboer, T.C.W., 2016. The right hemisphere is dominant in organization of visual search-A study in stroke patients. *Behavioural Brain Research* 304, 71–79. https://doi.org/10.1016/j.bbr.2016.02.004.

Ungerleider, L.G., Mishkin, M., 1982. Two cortical visual systems. In: Ingle, D.J., Goodale, M.A., Mansfield, R.J.W. (Eds.), *Analysis of Visual Behaviour*. MIT Press.

Vaina, L.M., 1989. Selective impairment of visual motion interpretation following lesions of the right occipito-parietal area in humans. *Biological Cybernetics* 61 (5), 347–359. https://doi.org/10.1007/BF00200800.

Van Dromme, I.C., Premereur, E., Verhoef, B.E., Vanduffel, W., Janssen, P., 2016. Posterior Parietal Cortex Drives Inferotemporal Activations During Three-Dimensional Object Vision. *PLOS Biology* 14 (4), e1002445. https://doi.org/10.1371/JOURNAL.PBIO.1002445.

Vossel, S., Weidner, R., Driver, J., Friston, K.J., Fink, G.R., 2012. Deconstructing the Architecture of Dorsal and Ventral Attention Systems with Dynamic Causal Modeling. *Journal of Neuroscience* 32 (31), 10637–10648. https://doi.org/10.1523/JNEUROSCI.0414-12.2012.

Wang, T., de Graaf, T., Tanner, L., Schuhmann, T., Duecker, F., & Sack, A. T. (2023). Hemispheric Asymmetry in TMS-Induced Effects on Spatial Attention: A Meta-Analysis. In *Neuropsychology Review*. Springer. https://doi.org/10.1007/s11065-023-09614-2.

Wang, W., Zhou, T., Chen, L., Huang, Y., 2023. A subcortical magnocellular pathway is responsible for the fast processing of topological properties of objects: A transcranial magnetic stimulation study. *Human Brain Mapping* 44 (4), 1617–1628. https://doi.org/10.1002/HBM.26162.

Warrington, E.K., Taylor, A.M., 1973. The Contribution of the Right Parietal Lobe to Object Recognition. *Cortex* 9 (2), 152–164. https://doi.org/10.1016/S0010-9452(73)80024-3.

Webster, K., Ro, T., 2017. Retinal and visual cortex distance from transcranial magnetic stimulation of the vertex affects phosphene perception. *Experimental Brain Research* 235 (9), 2857–2866. https://doi.org/10.1007/S00221-017-5022-4.

Whitwell, R.L., Sperandio, I., Buckingham, G., Chouinard, P.A., Goodale, M.A., 2020. Grip Constancy but Not Perceptual Size Constancy Survives Lesions of Early Visual Cortex. *Current Biology* 30 (18), 3680–3686.e5. https://doi.org/10.1016/j.cub.2020.07.026.

Xu, G.Q., Lan, Y., Zhang, Q., Liu, D.X., He, X.F., Lin, T., 2016. 1-Hz repetitive transcranial magnetic stimulation over the posterior parietal cortex modulates spatial attention. *Frontiers in Human Neuroscience* 10 (FEB2016). https://doi.org/10.3389/fnhum.2016.00038.

Xu, Y., 2018. The Posterior Parietal Cortex in Adaptive Visual Processing. In *Trends in Neurosciences* Vol. 41(11, 806–822.

Yao, D., 2001. A method to standardize a reference of scalp EEG recordings to a point at infinity. *Physiological Measurement* 22 (4), 693–711. https://doi.org/10.1088/0967-3334/22/4/305.